

GRAZ UNIVERSITY OF TECHNOLOGY



MASTER THESIS

---

# Optimization of sense coils for NFC test systems

---

*Author*  
B.W. AUER, BSc

*Supervisor*  
Ass.Prof. Thomas  
BAUERNFEIND



May 2020

## AFFIDAVIT

I declare that I have authored this thesis independently, that I have not used other than the declared sources/resources, and that I have explicitly indicated all material which has been quoted either literally or by content from the sources used. The text document uploaded to TUGRAZonline is identical to the present master's thesis dissertation.

29.05.2020

Date



Signature

## Kurzfassung

Near Field Communication (NFC) hat im täglichen Leben eine weite Verbreitung gefunden, wie z.B. beim kontaktlosen Zahlungsverkehr. Die Transponder im sogenannten Passive Communication Mode (Listener), welche für Zahlungsanwendungen verwendet werden, müssen die Interoperabilität mit bestehenden Point of Sales Terminals (Poller) und die Einhaltung des Standards gewährleisten. Diese Anforderungen werden in Labortests, bei welchen Fehler in der Kommunikation auftreten können, bestätigt. Im Falle eines Fehlers wird eine Messspule in das Betriebsvolumen eingesetzt um die Kommunikation zwischen Listener und Point of Sales Terminal zu überwachen. Diese Messung beeinflusst jedoch ihrerseits unweigerlich das zu vermessende System aus Poller und Listener. Deshalb ist es wünschenswert, einen physikalischen Aufbau zu finden, der die Beeinflussung durch das Messsystem auf ein Minimum reduziert. Dafür wurde mit dem Projektpartner der Messaufbau und ein Referenz Setup bestehend aus Poller und Listener spezifiziert und basierend auf den Spezifikationen, eine Vorstudie auf Basis von Finite-Elemente-Methode (FEM) Simulationen durchgeführt. Für die Optimierung der Sensorspulen-geometrie wurde schließlich das populationsbasierte Optimierungsverfahren der Differential Evolution (DE) eingesetzt. Das Vorwärtsproblem wurde mittels der Partial Element Equivalent Circuit (PEEC) Methode berechnet. Mit diesem Ansatz konnte so eine optimale Sensorspulen-geometrie für die spezifischen Anforderungen ermittelt werden.

## Abstract

Near field communication (NFC) has found widespread use in everyday life, such as in contactless payment applications. The listener devices (i.e. transponder cards in passive communication mode) used for such payment applications are required to provide interoperability with existing polling devices (i.e. point of sales terminals) and compliance with the standard. These requirements are confirmed in terms of measurements on prototypes in the laboratory. In case of erroneous communication, a measurement coil is inserted in the operating volume to monitor the communication between listener and poller. However, the measurement setup has an effect on the application environment. Therefore, it is desirable to find a physical measurement setup that minimizes the influence on the system consisting of listener and poller. The application environment of poller and listener as well as the measurement setup was defined together with the project partner, for which an optimal sense coil geometry was found. Based on these specifications a preliminary study in terms of finite element method (FEM) simulations was carried out. The optimization of the sense coil geometry relies on the differential evolution (DE) strategy. The forward problem was computed applying the partial element equivalent circuit (PEEC) method. Using this approach an optimal sense coil geometry for the specific requirements could be obtained.

# Contents

0.1	List of Abbreviations . . . . .	viii
<b>1</b>	<b>Introduction</b>	<b>1</b>
1.1	Problem Setting . . . . .	2
1.2	Thesis objectives . . . . .	2
1.3	Approach . . . . .	2
<b>2</b>	<b>Fundamentals</b>	<b>3</b>
2.1	NFC Fundamentals . . . . .	3
2.2	Multi-port theory . . . . .	4
2.3	PEEC Method . . . . .	7
2.4	Stochastic optimization . . . . .	8
<b>3</b>	<b>General specifications</b>	<b>10</b>
3.1	Operating volume . . . . .	10
3.2	Position of the sense coil . . . . .	12
3.3	Reference PICC/PCD . . . . .	12
3.4	Measurement setup . . . . .	12
<b>4</b>	<b>2D Approximation</b>	<b>14</b>
4.1	FEM Setup . . . . .	14
4.1.1	Geometry of Poller-0 . . . . .	16
4.1.2	Geometry of Listener-1 . . . . .	17
4.1.3	Coil positioning in z-direction . . . . .	17
4.2	Solving circuit and multi-port equations . . . . .	18
4.2.1	Matching circuit of Poller-0 . . . . .	19
4.2.2	Matching circuit of Listener-1 . . . . .	20
4.2.3	Solving Multi-port equations . . . . .	21
4.3	2D examinations . . . . .	24
4.3.1	Case 1- frequency behavior of $U_q$ considering no sense coil . . . . .	25
4.3.2	Frequency behavior of $U_q$ - considering sense coil influence . . . . .	26
<b>5</b>	<b>3D-Optimization</b>	<b>31</b>
5.1	Forward Problem - Partial equivalent element circuit method . . . . .	31
5.1.1	PEEC model of Poller-0 . . . . .	31

5.1.2	PEEC model of Listener-1 . . . . .	33
5.1.3	Testing compatibility with NFC Forum standard . . . . .	36
5.1.4	PEEC model of sense coil . . . . .	37
5.2	Formulation of the Optimization- Problem . . . . .	42
5.3	Optimization results . . . . .	43
5.3.1	Optimization process 1 . . . . .	44
5.3.2	Optimization process 2 . . . . .	49
5.3.3	Voltage excitation . . . . .	53
5.3.4	Optimization process 3 . . . . .	54
<b>6</b>	<b>Summary and outlook</b>	<b>59</b>

# List of Figures

1.1	Poller and listener configuration according to NFC Forum . . . . .	1
2.1	Mutual coupling of single loop coils . . . . .	3
2.2	Equivalent circuits for antenna coil structure . . . . .	4
2.3	T equivalent circuit of two inductively coupled coil . . . . .	5
2.4	Two-port building block . . . . .	6
2.5	Two-port building block . . . . .	6
2.6	Schematic of a PEEC stick element . . . . .	8
2.7	Flowchart of a basic DE algorithm . . . . .	9
3.1	EMVCo operating volume . . . . .	11
3.2	EMVCo test points . . . . .	12
3.3	Load impedance of sense coil consisting of cable and oscilloscope lumped elements . . . . .	13
4.1	Sectional view of the FEM setup . . . . .	15
4.2	Coil structure of Poller-0 . . . . .	16
4.3	Dimensions of Listener-1 . . . . .	17
4.4	Schematic representation of distances in z direction . . . . .	18
4.5	Matching circuit Poller-0 . . . . .	19
4.6	Equivalent matching-circuit for Poller-0 . . . . .	19
4.7	Principle sketch of circuit for NFC Forum listener devices . . . . .	20
4.8	Simplified matching circuit for Listener-1 . . . . .	21
4.9	Multi-port network with matching circuits, load impedance of sense coil and voltage source . . . . .	22
4.10	Circuitry of Poller-0 taking the inductive coupling to Listener-1 and sense into account . . . . .	24
4.11	Case 1 frequency behavior of $U_q$ . . . . .	25
4.12	Case 1 frequency behavior of the phase of $U_q$ . . . . .	26
4.13	Case 2 comparing the influence of different sense coils to the influence of Listener-1 TP 0 to TP 2 . . . . .	27
4.14	Case 2 comparing the influence of different sense coils to the influence of Listener-1 in TP 3 to TP 4 . . . . .	28
4.15	Case 3 comparing the influence of different sense coils to the influence of Listener-1 in TP 0 to TP 3 . . . . .	29

4.16	Case 3 comparing the influence of different sense coils to the influence of Listener-1 in TP 3 to TP 4 . . . . .	30
5.1	Poller-0 coil structure of PEEC model . . . . .	32
5.2	Matching circuit Poller-0 for PEEC model . . . . .	33
5.3	Geometry of Listener 1 for 3D-Optimization . . . . .	34
5.4	Change in input impedance of Listener-1 coil, depending on the number of stick elements used . . . . .	35
5.5	General coil geometry . . . . .	38
5.6	Example for the number of turns determination . . . . .	38
5.7	Exemplary sense coil structure . . . . .	39
5.8	Discretization example of coil geometry 1 . . . . .	41
5.9	Discretization example of coil geometry 2 . . . . .	41
5.10	Schematic coil positioning in Z-direction for 3D coil models . . . . .	43
5.11	Optimization process 1 convergence behavior of the geometry parameters and the return value "number of turns" . . . . .	45
5.12	Optimization process 1 convergence behavior of objectives and quality . . . . .	47
5.13	Optimization process 1 sense coil geometry for best solution . . . . .	48
5.14	Optimization process 2 convergence behavior of the geometry parameters and the return value "number of turns" . . . . .	50
5.15	Optimization process 2 convergence behavior of objectives and quality . . . . .	51
5.16	Optimization process 2 sense coil geometry for best solution . . . . .	52
5.17	Comparison of different voltage excitations . . . . .	53
5.18	Optimization process 3 convergence behavior of the geometry parameters and the return value "number of turns" . . . . .	56
5.19	Optimization process 3 convergence behavior of objectives and quality . . . . .	57
5.20	Optimization process 3 sense coil geometry for best solution . . . . .	58

# List of Tables

3.1	Coaxial cable and oscilloscope parameters . . . . .	13
4.1	Coordinates of test points used for the 2D approximation . . . . .	15
4.2	Values of geometric parameters for the 2D FEM model for Poller-0, Listener-1 and sense coil . . . . .	16
4.3	Obtained and reference values for PCD matching circuit . . . . .	20
4.4	Values of circuit components for Listener-1 matching . . . . .	21
4.5	Values of circuit components of multi-port circuitry . . . . .	22
5.1	Poller-0 geometrical parameters . . . . .	32
5.2	Obtained and reference values for PCD matching circuit . . . . .	33
5.3	Number of stick elements for Listener-1 . . . . .	35
5.4	Impedances of the 2D Listener-1 model with varying track width . . . . .	36
5.5	Summary of voltage values of the NFC Forum Reference Equipment Verification Tests . . . . .	37
5.6	Summary of voltage values of the NFC Forum Reference Equipment Verification Tests with asymmetrical voltage supply . . . . .	37
5.7	Overview coil structure creation method . . . . .	39
5.8	Summary of geometric parameters for the PEEC model of the sense coil . . . . .	40
5.9	EMVCo test points for optimization . . . . .	44
5.10	Optimization process 1 parameter space and best obtained solution . . . . .	44
5.11	Optimization process 1 values for fuzzy functions . . . . .	44
5.12	Optimization process 1 summary of geometric values for best solution . . . . .	48
5.13	Optimization process 2 parameter space and best obtained solution . . . . .	49
5.14	Optimization process 2 values for fuzzy functions . . . . .	49
5.15	Optimization process 2 summary of geometric values for best solution . . . . .	52
5.16	EMVCo test points for optimization process 3 . . . . .	54
5.17	Optimization process 3 parameter space and best obtained solution . . . . .	54
5.18	Optimization process 3 values for fuzzy functions . . . . .	55

## 0.1 List of Abbreviations

**PCD** Proximity Coupling Device

**PICC** Proximity Integrated Circuit Card

**NFC** Near field communication

**FEM** Finite Element Method

**RMS** Root Mean Square

**DE** Differential Evolution

**PEEC** Partial Element Equivalent Circuit

**EFIE** Electric Field Integral Equation

# Chapter 1

## Introduction

Near field communication (NFC) is a transmission protocol based on RFID (radio frequency identification). The technology has found widespread use in everyday life, such as access management in buildings, passports or payments. It is based on inductively coupled coils as illustrated in figure 1.1. There are at least two participants required, a poller<sup>1</sup> and listener<sup>2</sup>. The poller evokes an electromagnetic field through which data is transmitted from and to both devices. The listener can either be a passive device which is powered by the electromagnetic field of the poller, or an active one which carries its own power supply.

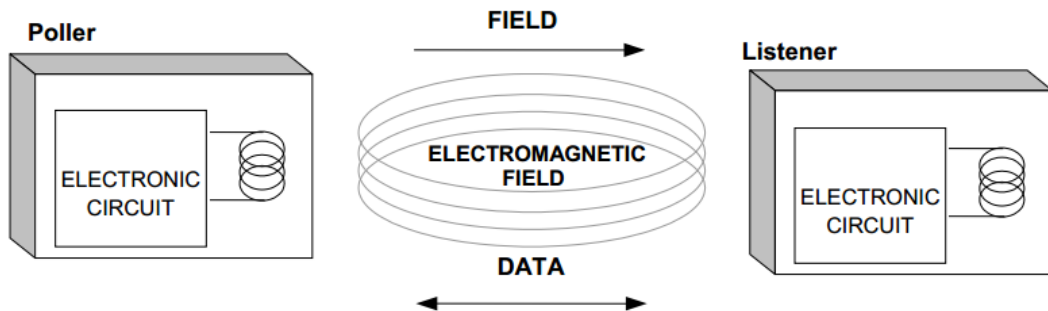


**Figure 1.1:** Poller and listener configuration according to NFC Forum ([1] page 10)

The operating range of NFC, is however, limited to a few centimetres due to the required inductively coupled coils. This contributes to security, but it might also cause issues during use if the listener is too far away or disturbances occur. In the process of development it is necessary to peruse the best possible performance while being compliant with corresponding standards to guarantee interoperability.

<sup>1</sup>In this document the terms poller, reader and PCD (Proximity Coupling Device as defined by ISO/IEC 14443) are used synonymously

<sup>2</sup>In this document the terms listener and PICC (Proximity Integrated Circuit Card as defined by ISO/IEC 14443) are used synonymously

## 1.1 Problem Setting

For listener devices which are used for payment applications interoperability with existing systems (terminals which act as polling devices) is desirable and compliance with the standard necessary. To confirm these requirements laboratory tests are carried out during which errors might be detected. In order to monitor the communication between the two devices in cases of error, a measurement coil (sense coil) will be inserted into the operating volume of the poller. This allows to potentially locate the cause of the error. However, in this environment the measurement setup has an influence on the application. Poller and listener form a resonant system which is detuned by the presence of the measurement system.

## 1.2 Thesis objectives

Due to the influence of the measurement on the application environment, it is desirable to find a physical setup of the measurement system which minimizes this effect. The main objective of this thesis is to find a sense coil geometry that minimizes the influence on the application environment so that the specifications of the project partner are met. These specifications are described in detail in chapter 3. The parameters for such a sense coil are synthesized in a optimization process.

## 1.3 Approach

Based on the specifications of the project partner, a preliminary study is carried out in terms of a 2D simulation of the problem. This is a fast way of collecting insights about the system to be examined.

In a second step the optimization of the sense coil geometry is performed. Therefore, an optimization strategy has to be chosen. Due to the lack of knowledge about the behaviour of the objective function in the multidimensional parameter space, stochastic optimization strategies are a good choice [2]. Therefore, the population based differential evolution strategy is applied. It follows the typical structure of evolutionary algorithms, but is characterized by a particular method for generating new candidate solutions [3].

For the computation of the forward problem the partial element equivalent circuit (PEEC) method is selected. It permits the treatment of lumped electric components and the discretized antenna structures in a single set of equations [4]. Additionally, it allows the computation of the forward problem with the required variety of sense coil geometries and is therefore ideal for the present task.

# Chapter 2

## Fundamentals

### 2.1 NFC Fundamentals

At the physical level NFC is a technology that is based on inductively coupled coils. It is operated at a frequency of 13.56 MHz within a operating distance of typically 3 cm to 5 cm [5]. For the communication between two NFC devices inductive coupling is required, for which loop antennas are used.

A common definition of the near field region is within a distance of  $\frac{\lambda}{2\pi}$  from the emitting antenna ([6] page 112-114), whereas  $\lambda$  is the wavelength of the electromagnetic wave. For NFC this amounts to:  $\frac{\lambda}{2\pi} = \frac{c}{f \cdot 2\pi} = 3.5 \text{ m}$ , whereas  $\lambda = 22.1 \text{ m}$ ,  $f$  refers to the operating frequency of 13.56 MHz and  $c$  to the speed of light.

Therefore, in a first approximation no wave propagation effects are considered. Hence, the two coils can be interpreted as a transformer, as is illustrated in figure 2.1.

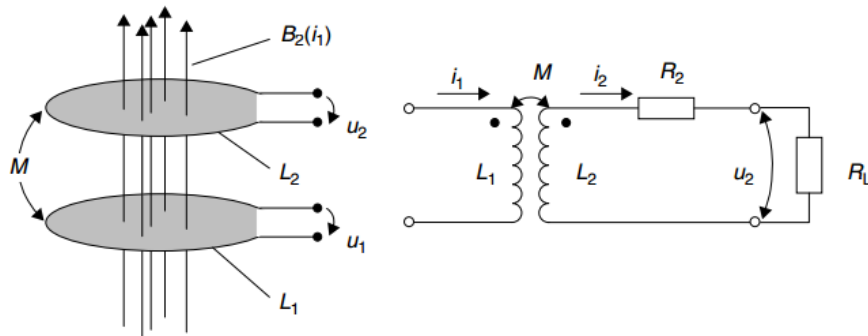


**Figure 2.1:** Mutual coupling of single loop coils ([6] page 73).  $L_1$  represents the poller coil and  $L_2$  the listener coil.  $R_2$  symbolizes the coil resistance and  $R_L$  represents a load.

In figure 2.1 the current  $i_1$  in coil  $L_1$  generates a time varying magnetic field which results in a time varying flux through coil  $L_2$ . This induces a voltage in coil  $L_2$ . The coils are coupled by the mutual inductance  $M$ .

Assuming that coil  $L_1$  acts as the poller antenna and coil  $L_2$  as the listener antenna of a NFC system, the following properties can be exploited. First, if the listener is passive, it can be powered by the electromagnetic field of the poller. Secondly, a change in  $i_2$  results in a change in  $i_1$  due to inductive coupling. This fact is used by listeners to respond to the poller ([1] page 10). The listener can either passively load the field of the poller or actively contribute ([7] page 12). The poller, on the other hand, "modulates the amplitude of its alternating magnetic field strength with modulation pulses" in order to transmit data to the listener ([7] page 12). For efficiency reasons both the poller and the listener are operated as resonant circuits. Therefore, a matching circuit is required that matches the resonant system (matching circuit and coil) to an resonant frequency of 13.56 MHz (page 73-74 [6]). In order to tune the loop antenna to the operating frequency, conjugate complex matching is required (page 73-74 [6]). Consequently, the input impedance of the antenna coil needs to be known.

The matching procedures relevant for this work are explained in more detail in section 4.2.1 and section 4.2.2.

The input impedance of an NFC antenna at the terminals is commonly described as an attenuated impedance. Depending on the knowledge about the antenna coil structure, the parasitic capacitance can be considered. Figure 2.2 shows two proposed equivalent circuits.

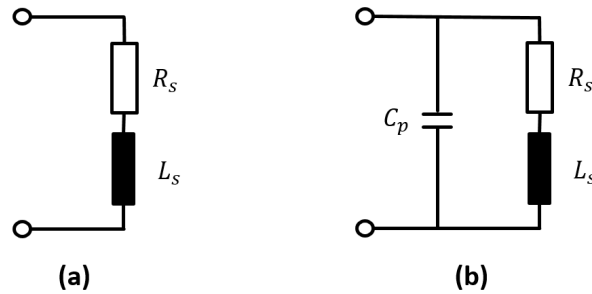


**Figure 2.2:** Equivalent circuits for antenna coil structure.  $R_s$  describes the ohmic losses of the antenna coil and  $L_s$  the inductance. In (b) the parasitic capacitance of the coil structure  $C_p$  is also considered [8].

## 2.2 Multi-port theory

As discussed in section 2.1, NFC is based on inductively coupled coils. In a first approximation, inductively coupled coils can be described by a T-equivalent circuit as shown in figure 2.3 ([9] page 787).

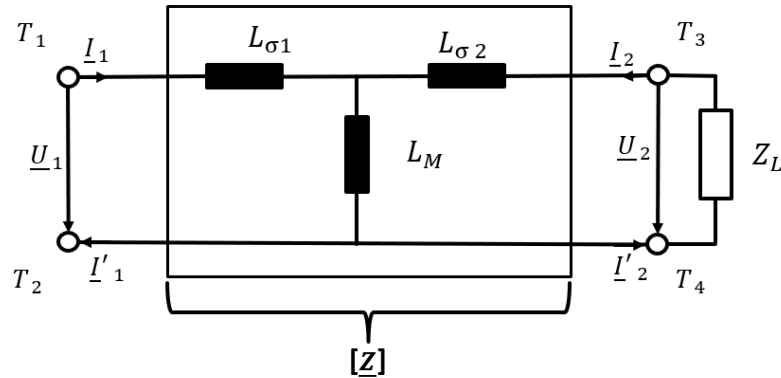


**Figure 2.3:** T equivalent circuit of two inductively coupled coils.  $L_M = M$ ,  $L_{\sigma 1} = L_1 - M$  and  $L_{\sigma 2} = L_2 - M$ , whereas the  $M$  represents the mutual inductance and  $L_1$  and  $L_2$  the respective self-inductances of the coils ([9] page 787).

One way of describing the transmission behavior of a circuit as the one shown in figure 2.3 is by interpreting it as a two-port. Multi-ports, or in this case two-ports, are a way of treating an electric circuit as a black box. The underlying idea is that only the terminal variables  $\underline{I}_1, \underline{U}_1, \underline{I}_2, \underline{U}_2$  are of interest, whereas the currents and voltages inside the circuit of the multi-port are not ([9] page 730). However, multi-ports are subject to a number of restrictions:

- It is applicable for linear, time invariant circuits ([10] page 368).
- No energy storages or independent sources are permitted within the circuit of the multi-port ([9] page 730).
- The terminal equations have to be fulfilled:  $\underline{I}_1 = \underline{I}'_1$  and  $\underline{I}_2 = \underline{I}'_2$  (page 730 [9]).
- No external connections between the ports are permitted. More specifically connections between the terminals  $T_1$  and  $T_3$  or  $T_4$  and connections between  $T_2$  to  $T_3$  or  $T_4$  ([9] page 730).

Figure 2.4 shows the building block of a two-port with the terminal variables. "The terminal pairs are referred to as port" (page 730 [9]).  $\underline{I}_1, \underline{I}'_1, \underline{I}_2, \underline{I}'_2$  represent the complex currents, whereas  $\underline{U}_1$  and  $\underline{U}_2$  represent the complex voltages at the ports.

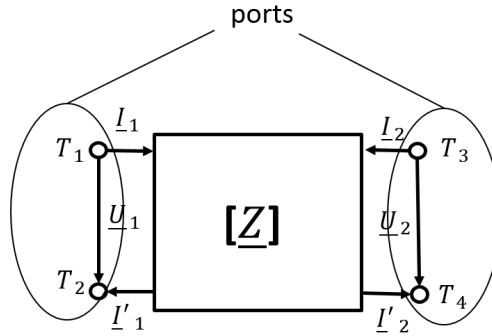


Figure 2.4: Two-port building block ([9] page 731)

One way of describing the electrical behavior of the multi-ports is by means of impedance-matrices ( $Z$ -matrices). The resulting linear multi-port matrix equation is given by ([11] page 13)

$$\begin{pmatrix} \underline{U}_1 \\ \underline{U}_2 \end{pmatrix} = \underbrace{\begin{bmatrix} \underline{Z}_{11} & \underline{Z}_{12} \\ \underline{Z}_{21} & \underline{Z}_{22} \end{bmatrix}}_{[\underline{Z}]} \begin{pmatrix} \underline{I}_1 \\ \underline{I}_2 \end{pmatrix}. \quad (2.1)$$

A typical application for the two port is shown in figure 2.5. The two port is driven by a source  $\underline{U}_s$  with a source resistance  $R_s$  and load  $\underline{Z}_L$  at port 2. The input impedance at port 1 is defined as  $\underline{Z}_{in} = \frac{\underline{U}_1}{\underline{I}_1}$  ([12] page 687).

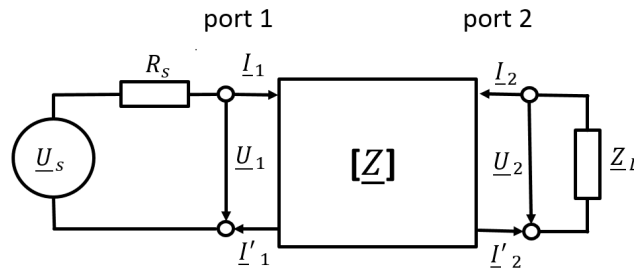


Figure 2.5: Two-port building block ([12] page 687)

The voltage at the ports is determined by the external circuitry due to ohms law. The voltage at port 2 is defined by  $\underline{U}_2 = -\underline{Z}_L \underline{I}_2$  and at port 1 by  $\underline{U}_1 = \underline{Z}_{in} \underline{I}_1$ . Hence, the two port equation result in:

$$\begin{pmatrix} \underline{Z}_{in} \underline{I}_1 \\ -\underline{Z}_L \underline{I}_2 \end{pmatrix} = \begin{bmatrix} \underline{Z}_{11} & \underline{Z}_{12} \\ \underline{Z}_{21} & \underline{Z}_{22} \end{bmatrix} \begin{pmatrix} \underline{I}_1 \\ \underline{I}_2 \end{pmatrix}. \quad (2.2)$$

Equation 2.2 can be solved for  $\underline{Z}_{in}$  which results in  $\underline{Z}_{in} = \underline{Z}_{11} - \frac{\underline{Z}_{12}\underline{Z}_{21}}{\underline{Z}_L + \underline{Z}_{22}}$  ([12] page 688). Therefore, the influence of the load  $\underline{Z}_L$  on the circuitry at port 1 can be determined.

## 2.3 PEEC Method

The numerical methods for solving Maxwell's equations can be roughly classified by methods which are based on the integral form - and those which are based on the differential form of Maxwell's equations. Methods that are based on the differential formulation require the discretization of the whole problem domain including air ([13] page 10 ). In contrast, solving methods which are based on the integral formulation only require the discretization of the conducting structures.

The partial element equivalent circuit method as introduced by Ruehli [14] is an integral based method for solving Maxwell's equations. In contrast to other integral equation based methods, it allows a circuit interpretation of the problem [15]. Consequently, it is a method to derive an equivalent electric circuit for the problem domain and then solve it by using SPICE like solving methods [15]. Therefore, the solution variables are expressed in the form of circuit variables. ([13] page 11).

In the applied implementation of the PEEC method, conducting structures are discretised into cylindrical one dimensional stick elements. In order to describe any stick element sufficiently, it is required to know its:

- Radius
- Length
- Specific resistance
- Position
- Connection to other elements

Due to the one dimensional character of the stick element, the current density within each stick element is constant. Hence, no proximity and skin effects can be taken into account. By using these stick elements the conducting structures are discretized. The air is not required to be discretized. Due to the free space Green's function  $G(\mathbf{r}, \mathbf{r}') = \frac{e^{-jk|\mathbf{r}-\mathbf{r}'|}}{|\mathbf{r}-\mathbf{r}'|}$  it is possible to obtain the electric field intensity for the whole problem domain by the electric field integral equation (EFIE). Equation 2.3 shows the EFIE for a configuration of  $K$  conductors [16].

$$\frac{\mathbf{J}(\mathbf{r}, \omega)}{\sigma} = \sum_{k=1}^K \frac{-j\omega\mu_0}{4\pi} \int_{\Omega_k} \mathbf{J}(\mathbf{r}', \omega) G(\mathbf{r}, \mathbf{r}') d\Omega' - \sum_{k=1}^K \frac{1}{4\pi\epsilon_0} \nabla \int_{\Omega_k} \rho(\mathbf{r}', \omega) G(\mathbf{r}, \mathbf{r}') d\Omega' \quad (2.3)$$

In equation 2.3  $\mathbf{J}$  represents the current density,  $\mathbf{r}$  the field point vector,  $\mathbf{r}'$  the source point vector,  $\omega$  the angular frequency,  $\rho$  the charge density,  $\mu_0$  the free space permeability and  $\epsilon_0$  the free space permittivity.

The EFIE is then solved by defining pulse series functions for the unknown currents and charge distribution [16]. The circuit interpretation can then be derived by following a method of moments process [16]. The resulting equations are then interpreted as circuit "resistive, inductive and capacitive voltage drops of a closed loop" ([13] page 83). The schematic circuit representation of a stick element is shown in figure 2.6.

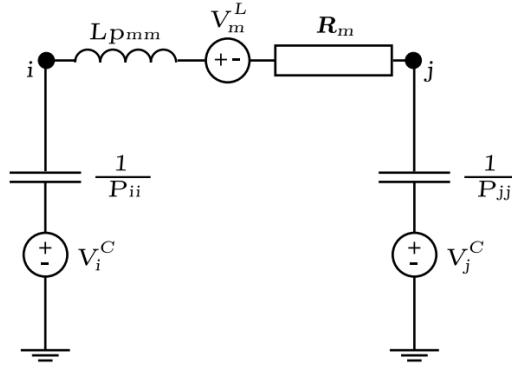


**Figure 2.6:** Schematic of a PEEC stick element. The stick element  $m$  connects the nodes  $i$  and  $j$ .  $Lp_{mmm}$  represents the partial self inductance of the stick element  $m$  and  $V_m^L$  accounts for the mutual inductance of all other stick elements to  $m$ .  $\frac{1}{P_{ii}}$  and  $\frac{1}{P_{jj}}$  are the partial self coefficients of the potential.  $V_i^C$  and  $V_j^C$  consider the mutual capacitive coupling from all other stick element to  $m$ .  $R_m$  represents the resistance of  $m$  by assuming a constant current density ([13] page 21-32).

If desired, circuits in form of concentrated lumped elements can easily be attached by adding appended nodes. For the modelling of NFC antennas this allows for the treatment of the antenna structure and matching circuitry in a single set of equations. Also the excitation can easily be handled within the matching circuits by adding voltage or current sources to the circuit equations [17].

## 2.4 Stochastic optimization

Deterministic optimization methods have been successfully applied to all fields of engineering. However, they do require the knowledge of certain properties of the objective function, such as convexity or differentiability, at least within a region surrounding the desired minimum. If no or very little is known about the objective function, it is advisable to use stochastic strategies. This is due to the fact that deterministic methods tend to converge towards a local minimum in such cases. Stochastic methods allow for the deterioration of objectives during the iteration process, which enables them to find the global optimum independently of the starting position of the strategy. In summary, stochastic strategies offer a stable "convergence and are able to find the desired region with a good probability"

[2]. However, they require a high number of function calls which makes them computation intensive [2].

For the present task the differential evolution (DE) strategy is selected. The DE strategy is based on the typical structure of an evolutionary algorithm, but employs a particular method to generate new candidate solutions [3]. Evolutionary strategies try to mimic the organic evolution for optimum seeking [2]. Figure 2.7 shows the process for a basic DE algorithm in form of a flow chart.

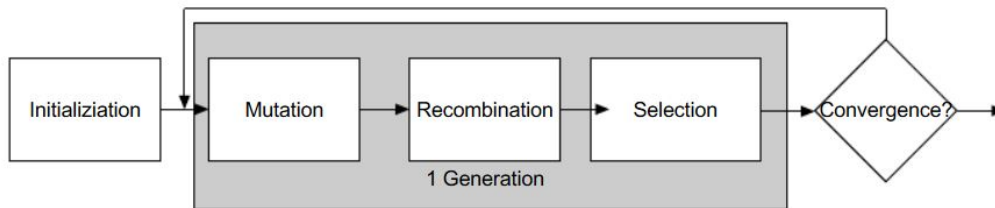


**Figure 2.7:** Flowchart of a basic DE algorithm [3]

First, the individuals are randomly initialized within the parameter space. Then a sequence of steps is taken, referred to as generation, until a convergence criteria is satisfied, for example the maximum number of iterations is reached. After initialization, the population (all individuals) is subject to mutation which results in the exploration of the parameter space. Then the parameters of the mutated individuals are mixed with the parameters of donor individuals (previously successful individuals). Therefore, previously successful features are reused. This results in the generation of trial individuals which are then subject to selection, mimicking the survival of the fittest process in nature [3].

## Chapter 3

# General specifications

In this chapter the general specifications are presented, which were determined in accordance with CISC- Semiconductor. They apply to all following examinations, unless stated otherwise, and are structured in the following way:

- Operating volume
- Position of the sense coil
- Reference poller and listener
- Measurement Setup

### 3.1 Operating volume

Due to the fact that ISO IEC 14443 leaves the definition of the operating volume to PCD manufacturers, there are different operating volumes to choose from. Both EMVCo and the NFC Forum define operating volumes. In accordance with the project partner the decision was made to apply the volume defined by EMVCo. It is displayed in figure 3.1

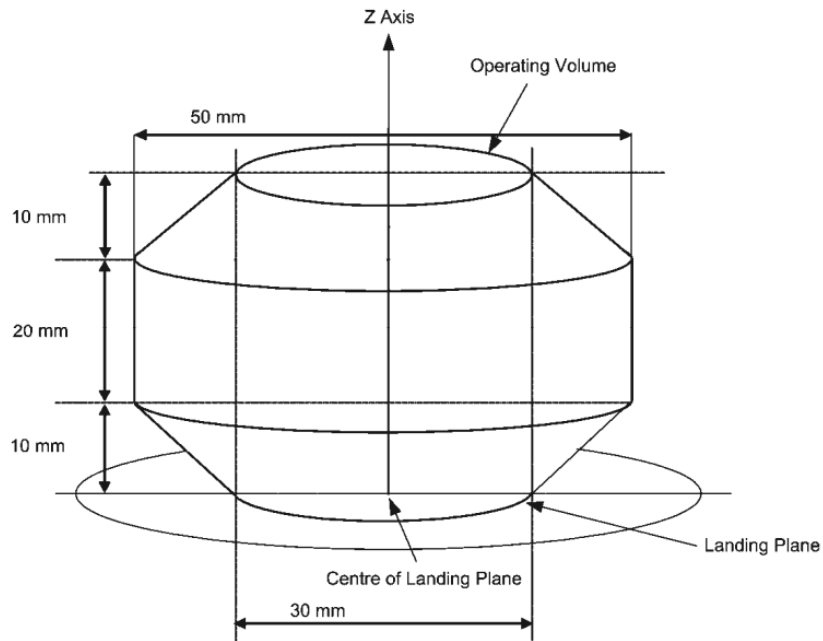


**Figure 3.1:** EMVCo operating volume [18]

The test points are defined by EMVCo as follows [18]: In Z-direction the operating volume is divided into 5 test plains at 0 cm, 1 cm, 2 cm, 3 cm and 4 cm distance from the landing plane. Figure 3.2 shows the test points in the test plains at a distance of 10 mm to 30 mm from the landing plane. For the other test plains the test points at 25 mm from the centre are not considered as is apparent from figure 3.1.

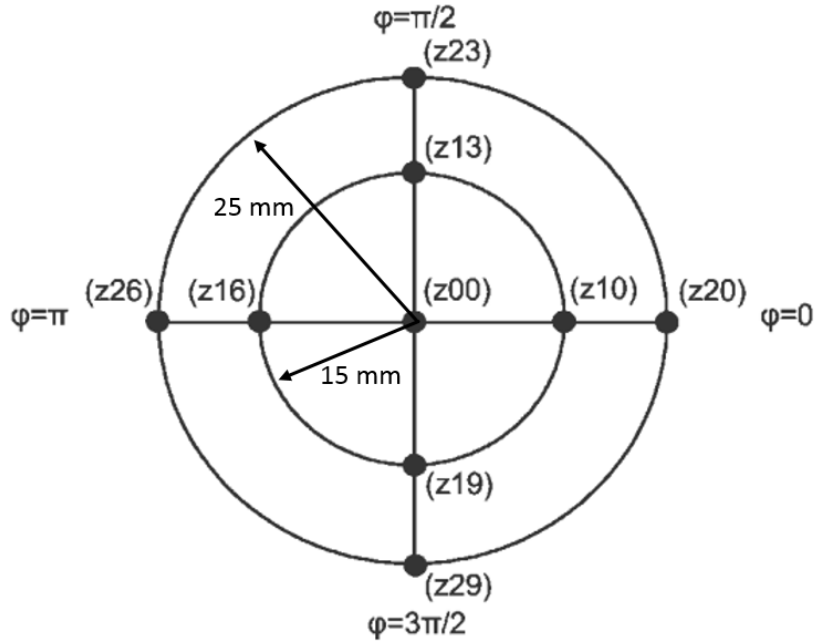


**Figure 3.2:** EMVCo test points for test plains at a distance of 10 mm and 20 mm from the landing plane [18].

## 3.2 Position of the sense coil

Generally, there are no restrictions concerning the placement of sense coil. However, in the laboratory setup the PICC has to move in the operating volume which makes it impractical to place the sense coil directly in the volume.

## 3.3 Reference PICC/PCD

It was specified that PICCs of Class 1 according to ISO-14444-1 should be investigated. More specifically, the NFC- Forum Listener-1 was selected as a representative PICC since it complies with ISO Class 1 and is generally used as a reference device. As a representative PCD, Poller-0 of the NFC Forum was chosen. Both in accordance with CISC-Semiconductor.

## 3.4 Measurement setup

In accordance with the project partner, it was specified that the measurement setup should consist of a 2 m long coaxial cable and an oscilloscope.

A transmission line, such as a coaxial cable, can be considered electrically short if the line length does not exceed a tenth of the smallest wavelength [19]. As can be seen in equation 3.1,  $\lambda$  at 13.56 MHz is still one decade larger than the cable length  $l_{cable}$ . Therefore, the cable can be modelled by lumped elements and no wave propagation effects have to be taken into account. For this purpose, it is assumed to be a loss-free cable.

$$\lambda = \frac{c}{f} = 22.1 \text{ m} > 10 * l_{cable} = 20 \text{ m} \quad (3.1)$$

The oscilloscope is modelled with its input impedance consisting of an input resistance  $R_{oszi}$  and input capacitance  $C_{oszi}$ . The resulting circuit acting as load for the sense coil is displayed in figure 3.3. One specification of the project partner concerning the sense coil was that it should produce a voltage at the input of the oscilloscope  $\underline{U}_{sense}$  higher than a certain minimum level. Therefore, the magnitude of  $\underline{U}_{sense}$  is considered for levels higher than 10 mV and 15 mV.

The values of the lumped element in figure 3.3 are summarized in table 3.1. The values displayed in table 3.1 were determined in accordance with the project partner.

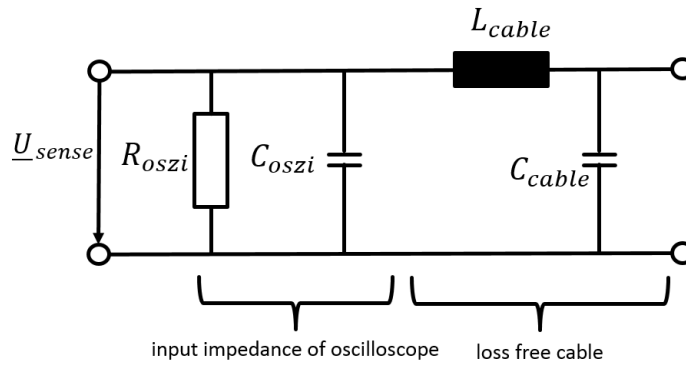


**Figure 3.3:** Load impedance of sense coil consisting of cable and oscilloscope lumped elements.  $C_{cable}$  is the capacitance and  $L_{cable}$  the inductance of the 2 m coaxial cable. The input impedance of the oscilloscope is comprised of  $R_{oszi}$  and  $C_{oszi}$ .

Parameter	Value
$C_{cable}$	190.3 pF
$L_{cable}$	439.6 nH
$C_{oszi}$	15 pF
$R_{oszi}$	1 M $\Omega$

**Table 3.1:** Coaxial cable and oscilloscope parameters

## Chapter 4

# 2D Approximation

In this chapter the preliminary study is described. The aims of this study are to collect insights about the system to be examined. To achieve this goal, a two-dimensional rotational symmetrical FEM model of the setup was built and evaluated.

The proprietary FEM-based software "EleFAnT2D" was applied. A direct coupling of the modelled coil structure and the required matching circuits is not implemented. Therefore, "EleFAnT2D" was used to compute the impedance matrices of the setup. In the following, the matching circuits are modelled in MATLAB by solving the circuit equations, as well as the corresponding multi-port equations.

### 4.1 FEM Setup

The proprietary software "EleFAnT2D" allows the computation of two dimensional axis symmetrical time harmonic eddy current problems. Due to the axis symmetrical requirement, only curricular coil structures can be modelled. The coil structure of Listener-1 is therefore transformed by maintaining the inner surface area as described in section 4.1.2. Since the coil structure of Poller-0 is circular, as can be seen in figure 4.1, no such transformation was needed.

Another constraint of the chosen approach is that horizontal shifts in position between the coils can not be examined. This constraint is a result of the requirement of the axis symmetry, since a horizontal shift would require a shift in the r dimension (see figure 4.1) which would result in a change of coil geometry. Therefore, only the central positions of the EMVCo operating volume are investigated, which are summarized as test points ( $TP$ ) in table 4.1.

Due to the assumed negligible effect of the substrate, it is not taken into account. Its effect on coil position in z-direction is considered and described in section 4.1.3. The material of the conducting structures is modelled as copper with a conductivity of  $5.7 \cdot 10^7 \frac{S}{m}$ . The simulation setup can be seen in figure 4.1 (topological view of the problem area). It displays the sectional view of the FEM problem. The coils of Listener-1 and Poller-0 each consist

Test point	Value in x, y, z -direction in mm
TP 0	0, 0, 0
TP 1	0, 0, 10
TP 2	0, 0, 20
TP 3	0, 0, 30
TP 4	0, 0, 40

**Table 4.1:** Coordinates of test points used for the 2D approximation

of 4 turns (of which Poller-0 has only two active turns), the sense coil is assumed to have one turn. The geometry of each turn is defined by its conductor thickness  $h_c$ , conductor width  $CT$  and its distance to the symmetry axis  $r$ , which determines the coil's radius. The values of these parameters are summarized in table 4.2 for Listener-1, Poller-0 and sense coil. The conductor thickness  $h_c$  is assumed to be  $35 \mu m$  for all conducting structures.

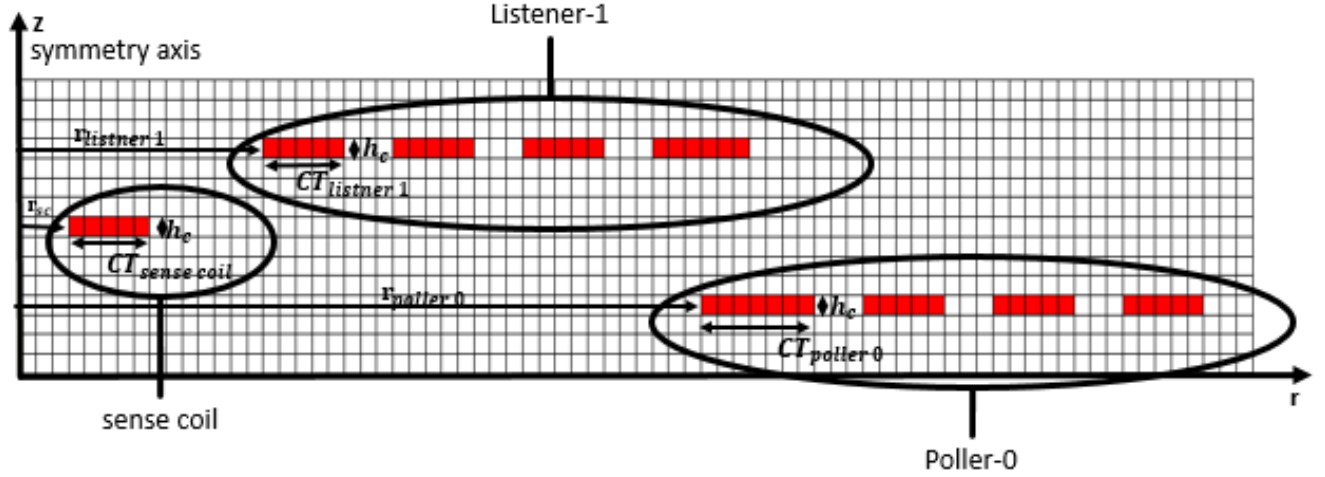


**Figure 4.1:** Sectional view of the FEM setup. The grid in the background refers to the macro elements. Since the last turn of Listener-1 overlaps in the  $r$  dimension with the first turn of Poller-0, the first turn of Poller-0 required more macro elements. The macro elements were chosen in a way that the coil geometry is not affected.

At 13.56 MHz the penetration depth  $\delta$  caused by the skin effect results in  $\delta = \sqrt{\frac{2 * \rho}{\omega \mu}} = 18,103 \mu m$ .  $\rho$  is the specific resistance,  $\omega$  the angular frequency and  $\mu$  the magnetic permeability of copper. This provides certain challenges for modelling, since areas with high current densities require more careful discretization to provide sufficiently precise simulation results. However, the distance between Poller-0 and Listener-1 stretches up to 4 cm. Hence, an appropriate discretization is required. Therefore, areas where high field strength changes occur (such as the edge of conductors), are discretised using a higher density of finite elements than areas with lower changes in field strength.

Parameter	Value
$h_c$	$35 \mu m$
$r_{listener1}$	$27.2 mm$
$r_{sc}$	$10 mm, 25 mm, 40 mm$
$r_{Poller0}$	$30.5 mm$
$CT_{sensecoil}$	$0.5 mm$
$CT_{Listener1}$	$0.5 mm$
$CT_{Poller0}$	$1 mm$

**Table 4.2:** Values of geometric parameters for the 2D FEM model for Poller-0, Listener-1 and sense coil

#### 4.1.1 Geometry of Poller-0

Poller-0 was modelled according to the specifications of the NFC-Forum. The main coil structure of Poller-0 is found at the mid layer 1 which is displayed in figure 4.2.

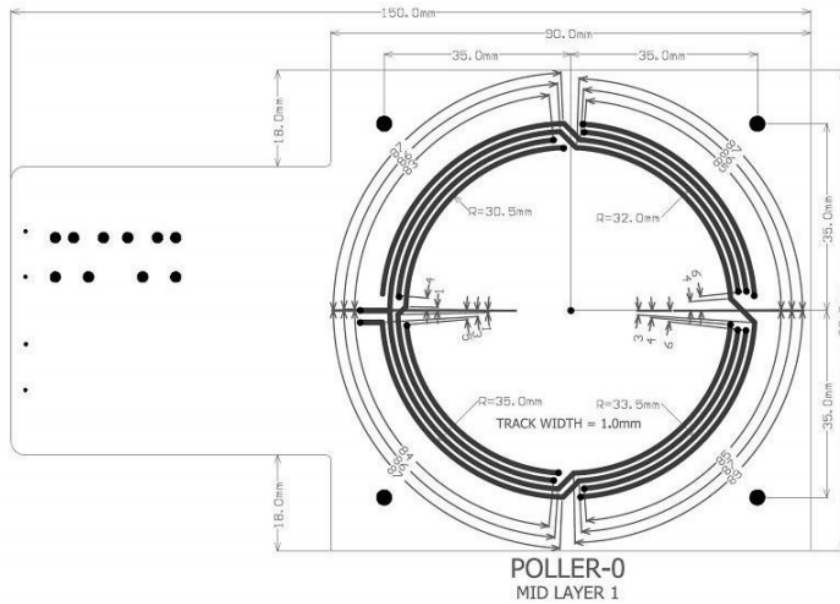


**Figure 4.2:** Coil structure of Poller-0 ([1] page 85)

As can be seen in figure 4.2, the track width of Poller-0 is  $CT_{Poller-0} = 1 mm$ . The tracks are each  $0.5 mm$  apart and have therefore the resulting radii. Due to the fact that the coil structure is electrically compensated, in the FEM model the outer two turns are operated as open circuited. Hence these two turns (see figure 4.1 Poller-0) are modelled as one coil with no load. The inner two turns are treated as the input current carrying coil. Consequently, the inner two tracks are treated as a coil with 2 turns carrying the input current, and the outer 2 tracks are seen as a different coil with two turns with the

condition that the total current is zero.

### 4.1.2 Geometry of Listener-1

The main coil structure of Listener-1 is found at the top layer, as displayed in figure 4.3. The track width of Listener-1  $CT_{Listener-1} = 0.5 \text{ mm}$  and the tracks are  $0.5 \text{ mm}$  apart from each other.

In contrast to Poller-0, Listener-1 is a rounded rectangular antenna. As a consequence, the antenna has to be transformed into a circular coil structure. This can be done by maintaining the inner surface area of the antenna coil, resulting in a radius for the inner edge of the inner track of  $27.2 \text{ mm}$ . The maintenance of the surface area attempts to minimize the error in flux, but accepts an error made in losses. The losses in the coil are depended on the conductor length which is altered in order to maintain the surface area of the coil.

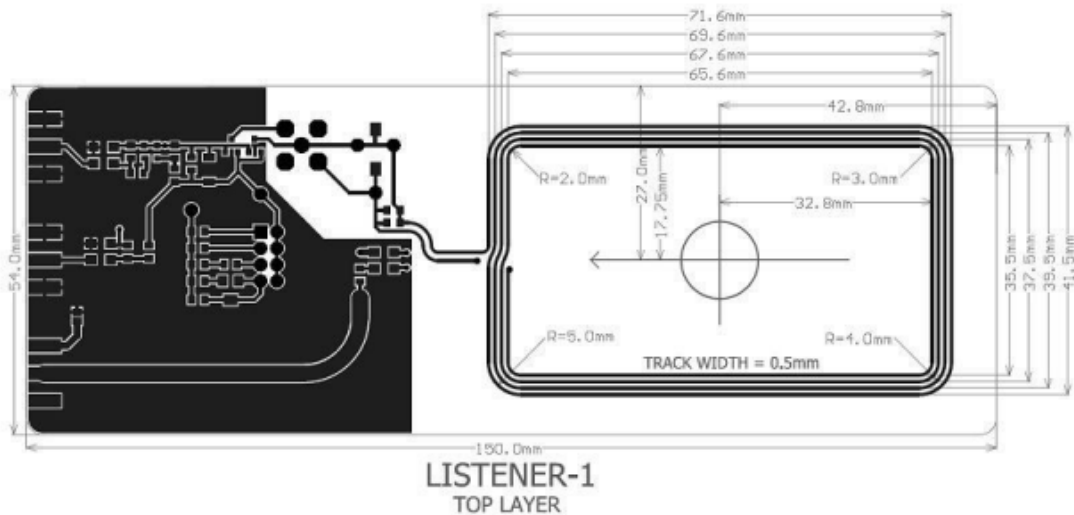
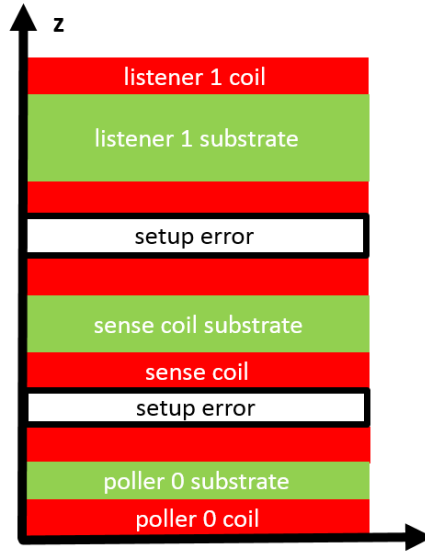


Figure 4.3: Dimensions of Listener-1 ([1] page 91)

### 4.1.3 Coil positioning in z-direction

The distance between the conducting structures in z-direction is mainly driven by the thickness of the substrate. Figure 4.4 shows a schematic representation of the coil structure in z-direction. Substrates are marked green, conductors red and the assumed setup error white. Conducting structures are assumed to have a thickness of  $35 \mu\text{m}$  (see table 4.2) and the setup error with  $0.25 \text{ mm}$ . In laboratory testing conditions placing the coils exactly on top of each other might not be possible, therefore the setup error is assumed. In reality, all three coils are built up by a 3D structure, resulting in different layers for construction. For Poller-0 there are 4 layers specified by the NFC Forum. Most of the coil structure of

Poller-0, however, is found in mid layer 1 ([1] page 85). This leaves the displayed substrate thickness of Poller-0 in figure 4.4 with  $0.22\text{ mm}$ . The sense coil substrate is assumed to be  $0.4\text{ mm}$  thick with the main coil structure on the bottom and bridges at the top. The substrate thickness of Listener-1 is  $0.8\text{ mm}$  with the main coil structure at the top layer as specified by the NFC Forum.



**Figure 4.4:** Schematic representation of distances in  $z$  direction

Using this setup, the impedance matrices are computed. For the following examinations the change in inductive coupling between the coils is relevant which changes for each test point in  $z$ -direction (see table 4.1) and each radius  $r$  of sense coil examined. Hence, a large number of simulations is required.

## 4.2 Solving circuit and multi-port equations

In order to model Poller-0 and Listener-1 according to the requirements of the NFC Forum, matching both antenna coils to  $13.56\text{ MHz}$  with their respective matching circuits is necessary. Therefore, the coil impedances of Poller-0 and Listener-1 were computed, assuming that no other coils are present as required by the NFC Forum ([1] page 67-70). The antenna coil impedances obtained by the FEM simulation are interpreted as an inductivity with serial losses, since capacitive effects are neglected by the 2D axis symmetrical model. The matching procedures applied are described in detail in section 4.2.2 and section 4.2.1.

### 4.2.1 Matching circuit of Poller-0

In the following section the simplifications and modelling of the matching circuit for Poller-0 are described, while complying to the requirements of the NFC Forum[1]. The resulting component values are given in table 4.3

Since the resonance frequency of Poller-0 coil is not 13.56 MHz, a matching circuit is required as shown in 4.5. The procedure for fine-tuning is described in B.5 of [1]. For calibration and use it is required that socket J2 of Poller-0 is terminated with a 50 Ω resistor. Additionally, the input impedance at J1 has to be 50 Ω if correctly tuned and matched at 13.56 MHz.

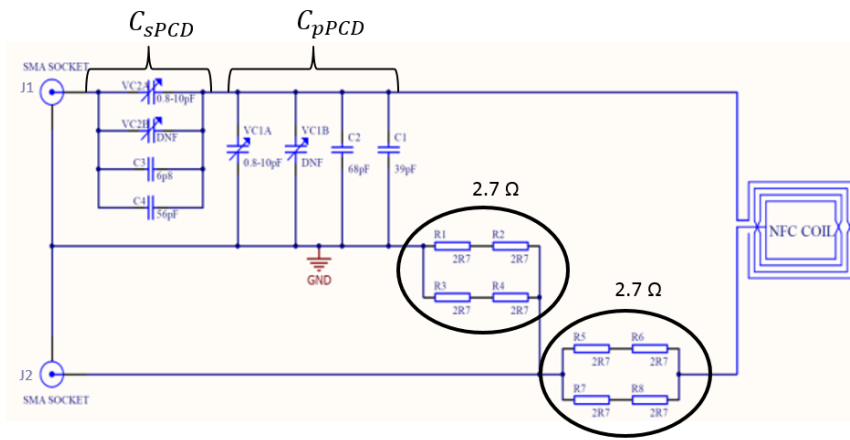


**Figure 4.5:** Matching circuit Poller-0 ([1] page 74)

The requirements of the NFC Forum lead to a simplified matching circuit for Poller-0 as shown in figure 4.6. The value of  $R_E$  can be calculated considering the component values on page 78 [1] and the 50 Ω resistor at J2. For tuning and matching it is required that  $C_{pPCD}$  and  $C_{sPCD}$  are chosen in such a way that  $Z_{inPCD} = 50 + j0 \Omega$ .

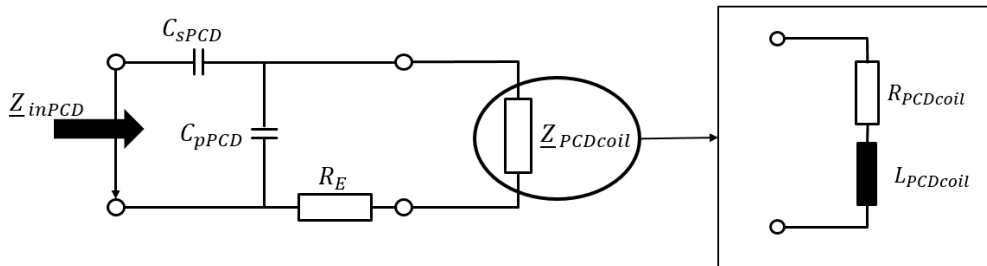


**Figure 4.6:** Equivalent matching-circuit for Poller-0.  $R_{PCDcoil}$  represents the ohmic losses of the Poller-0 antenna coil and  $L_{PCDcoil}$  the inductance.

In order to solve the circuit equations, the input impedance of the Poller-0 antenna coil

Circuit components	Obtained Values	NFC Forum reference range
$C_{sPCD}$	74.39 pF	63.6 pF - 72.8 pF
$C_{pPCD}$	139.93 pF	107.8 pF - 117 pF
$R_E$	5.2617 $\Omega$	5.2617 $\Omega$
$R_{PCDcoil}$	0.515 $\Omega$	-
$L_{PCDcoil}$	65.680 $\mu H$	-

**Table 4.3:** Obtained and reference values ([1] page 78) for PCD matching circuit.

$\underline{Z}_{PCDcoil}$  has to be known. For this purpose "EleFAnT2D" was used to obtain  $\underline{Z}_{pcd} = R_{PCDcoil} + j\omega L_{PCDcoil} = 0.515 + j55.96 \Omega$ . The setup used to obtain  $\underline{Z}_{pcd}$  assumes that no other coils are present, as required by the NFC Forum ([1] page 67-70). Consequently, the circuit equations for the matching-circuit in figure 4.6 can be solved, so that  $\underline{Z}_{inPCD} = 50 + j0 \Omega$  resulting in the values for  $C_{pPCD}$  and  $C_{sPCD}$  displayed in table 4.3.

As can be seen in table 4.3 the obtained values for  $C_{sPCD}$  and  $C_{pPCD}$  are close to the range of values specified by the NFC Forum. Since  $C_{sPCD}$  and  $C_{pPCD}$  depend on the impedance of the coil structure of Poller-0  $\underline{Z}_{PCDcoil}$ , a deviation from the NFC Forum reference values is expected. Due to the fact that the axis symmetrical model neglects capacitive effects, it is expected that the obtained values for  $C_{sPCD}$  and  $C_{pPCD}$  are higher than the reference values by the NFC Forum. Additionally, the coil structure of Poller-0 was simplified as described in section 4.1.1 which also contributes to the error made in the calculation of  $\underline{Z}_{PCDcoil}$ .

#### 4.2.2 Matching circuit of Listener-1

The circuits for NFC Forum listeners are defined in ([1] page 79-84). Figure 4.7 shows the principle sketch of this circuitry. As can be seen in figure 4.7, the listener coil is connected to a tuning capacitance  $C_{res}$ , followed by a bridge rectifier which is loaded with the test resistance  $R_Q$  [17]. The test resistance  $R_Q$  is set depending on the test case ([1] page 54-63). The NFC Forum defines multiple load cases for its listener devices. Two cases are with  $R_Q = 820 \Omega$  and  $R_Q = 82 \Omega$  in order to test the power transfer from reader to listener([1] page 54) - the so called power requirement test. For the purpose of this work, the two values for  $R_Q$  of the power requirement test are considered.

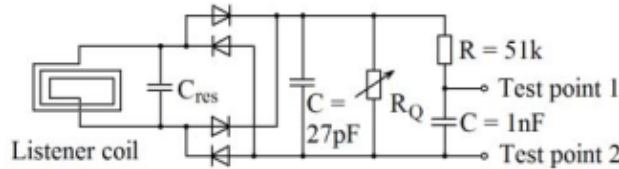


**Figure 4.7:** Principle sketch of circuit for NFC Forum listener devices [17].  $R_Q = 820 \Omega$  for Hmin and  $R_Q = 82 \Omega$  for Hmax ([1] page 54-63)

The power requirement test of the NFC Forum differentiates between two cases for which

different loads are applied [20].

- Hmax case: the voltage at the test resistance must not exceed the voltage level as described in [1].
- Hmin case: the voltage level at the test resistance must exceed the lower limit as described in [1].

As proposed in [21], the bridge rectifier can be modelled in terms of a linear resistance in order to allow for frequency domain examinations. The value of the linear resistance (in the following referred to as  $R_{LPICC}$ ) was obtained in [21] by fitting measurements of a standardised polling device, utilizing a least square approximation. Based on the results of [21], the matching circuit of Listener-1 was simplified to the circuit shown in figure 4.8.

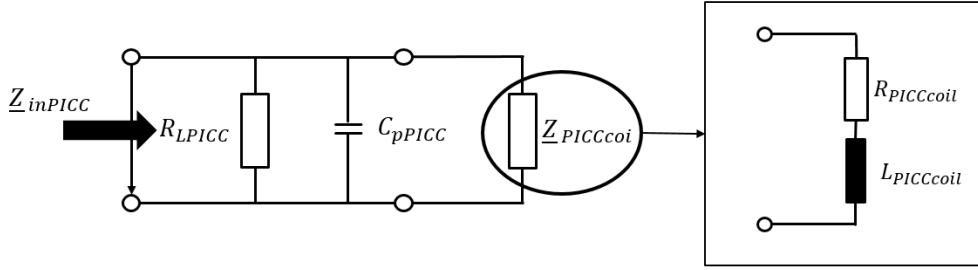


**Figure 4.8:** Simplified matching circuit for Listener-1.  $L_{PICCcoil}$  represents the inductance and  $R_{PICCcoil}$  the ohmic losses of the antenna coil of Listener-1.

Circuit components	Values of circuit components
$C_{sPICC}$	65.553 pF
$R_{LPICC}$	Hmin = 450 $\Omega$ , Hmax = 50 $\Omega$ [21]
$L_{PICCcoil}$	2.1014 $\mu H$
$R_{PICCcoil}$	1.26 $\Omega$

**Table 4.4:** Values of circuit components for Listener-1 matching

The impedance of the Listener-1 coil  $Z_{PICCcoil} = R_{PICCcoil} + j\omega L_{PICCcoil}$  was computed by applying "EleFAnT2D", under the condition that no other coils are present. In order to model the matching procedure described by the NFC Forum,  $C_{pPICC}$  was chosen so that  $Im\{Z_{inPICC}\} = 0$  at operating frequency. The values for the circuit components of figure 4.8 are summarized in table 4.4.

### 4.2.3 Solving Multi-port equations

In the following examinations, the influence of an sense coil on the resonant system of Poller-0 and Listener-1 is investigated. Therefore, the change in  $U_q$  is examined depending on the following conditions:

- distance to landing plane see section 4.1
- sense coil radius
- load impedance of sense coil

Consequently, the value of  $\underline{U}_q$  has to be obtained. The starting point for the calculations are the required Z-matrices and the values for the matching circuits of Poller-0 and Listener-1 as well as the value for  $\underline{Z}_{sense}$ . In essence, the entries for the Z-matrix of the multi- port and the loads at ports 2 and 3 have to be known. The resulting multi- port problem is shown in figure 4.9.

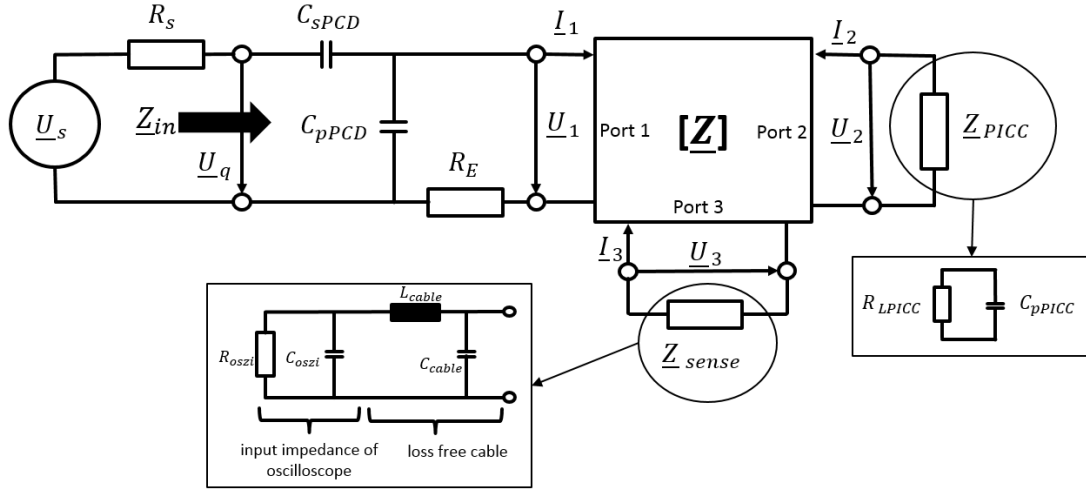


**Figure 4.9:** Multi-port network with matching circuits, load impedance of sense coil and voltage source. Poller-0 is excited by a voltage source  $\underline{U}_s$  with a source resistance  $R_s$ . The matching circuit of Poller-0 can be found between the voltage source and port 1. The load impedances for Listener-1  $\underline{Z}_{PICC}$  and the sense coil  $\underline{Z}_{sense}$  are found at ports 2 and 3 respectively.

Circuit components	Values
$R_s$	50 $\Omega$ ([22] page 5-7)
$\underline{U}_s$	5 V <sub>p</sub> at 13.56MHz ([22] page 5-7)
$C_{sPCD}$	74.39 pF
$C_{pPCD}$	139.93 pF
$R_E$	5.2617 $\Omega$
$C_{pPICC}$	65.553 pF
$R_{LPICC}$	Hmin = 450 $\Omega$ , Hmax = 50 $\Omega$
$C_{cable}$	190.3 pf
$L_{cable}$	439.6 nH
$C_{oszi}$	15 pF
$R_{oszi}$	1 M $\Omega$

**Table 4.5:** Values of circuit components for multi-port circuitry

For the present task it is of interest to determine the influence of  $\underline{Z}_{sense}$  and  $\underline{Z}_{PICC}$  on the circuitry at Port 1. One way of doing this is to calculate the input impedance at Port 1 taking into account the loads at the other two ports  $\underline{Z}_{sense}$  and  $\underline{Z}_{PICC}$ . By definition, the input impedance of a multi-port is given by  $\underline{Z}_E = \frac{U_1}{I_1}$ . When  $\underline{Z}_E$  is known, the resulting circuit, as shown in figure 4.10, can easily be solved by solving the circuit equations.

The multi-port can be described by a set of linear equation  $\underline{U} = [\underline{Z}]\underline{I}$  with

$$\underline{U} = \begin{pmatrix} \underline{U}_1 \\ \underline{U}_2 \\ \underline{U}_3 \end{pmatrix}, \underline{I} = \begin{pmatrix} \underline{I}_1 \\ \underline{I}_2 \\ \underline{I}_3 \end{pmatrix}, \text{ and } [\underline{Z}] = \begin{bmatrix} \underline{Z}_{11} & \underline{Z}_{12} & \underline{Z}_{13} \\ \underline{Z}_{21} & \underline{Z}_{22} & \underline{Z}_{23} \\ \underline{Z}_{31} & \underline{Z}_{32} & \underline{Z}_{33} \end{bmatrix}$$

where  $\underline{U}$  and  $\underline{I}$  are unknown. Since the loads at ports 2 and 3 are known, the multi-port equations can be expressed as:

$$\begin{pmatrix} \underline{U}_1 \\ -\underline{Z}_{PICC}\underline{I}_2 \\ -\underline{Z}_{sense}\underline{I}_3 \end{pmatrix} = \begin{bmatrix} \underline{Z}_{11} & \underline{Z}_{12} & \underline{Z}_{13} \\ \underline{Z}_{21} & \underline{Z}_{22} & \underline{Z}_{23} \\ \underline{Z}_{31} & \underline{Z}_{32} & \underline{Z}_{33} \end{bmatrix} \begin{pmatrix} \underline{I}_1 \\ \underline{I}_2 \\ \underline{I}_3 \end{pmatrix}. \quad (4.1)$$

Then the terms  $-\underline{Z}_{PICC}\underline{I}_2$  and  $-\underline{Z}_{sense}\underline{I}_3$  can be moved to the right hand side resulting in:

$$\begin{pmatrix} \underline{U}_1 \\ 0 \\ 0 \end{pmatrix} = \begin{bmatrix} \underline{Z}_{11} & \underline{Z}_{12} & \underline{Z}_{13} \\ \underline{Z}_{21} & \underline{Z}_{22} + \underline{Z}_{PICC} & \underline{Z}_{23} \\ \underline{Z}_{31} & \underline{Z}_{32} & \underline{Z}_{33} + \underline{Z}_{sense} \end{bmatrix} \begin{pmatrix} \underline{I}_1 \\ \underline{I}_2 \\ \underline{I}_3 \end{pmatrix}. \quad (4.2)$$

By following the approach to reduce the number of ports as described in [23] (page 58-65) the input impedance  $\underline{Z}_E$  can be obtained as follows. By rewriting (4.2) as

$$\begin{pmatrix} \underline{U}_1 \\ 0 \end{pmatrix} = \begin{bmatrix} \underline{Z}_{11} & \tilde{\underline{Z}}_{12} \\ \tilde{\underline{Z}}_{21} & \tilde{\underline{Z}}_{22} \end{bmatrix} \begin{pmatrix} \underline{I}_1 \\ \tilde{\underline{I}}_2 \end{pmatrix} \quad (4.3)$$

where

$$\tilde{\underline{I}}_2 = \begin{pmatrix} \underline{I}_2 \\ \underline{I}_3 \end{pmatrix}, \tilde{\underline{Z}}_{12} = [ \underline{Z}_{12} \quad \underline{Z}_{13} ], \tilde{\underline{Z}}_{21} = \begin{bmatrix} \underline{Z}_{21} \\ \underline{Z}_{31} \end{bmatrix}, \text{ and } \tilde{\underline{Z}}_{22} = \begin{bmatrix} \underline{Z}_{22} + \underline{Z}_{PICC} & \underline{Z}_{23} \\ \underline{Z}_{32} & \underline{Z}_{33} + \underline{Z}_{sense} \end{bmatrix}$$

4.3 can then be solved for  $\underline{Z}_E = \frac{U_1}{I_1}$  resulting in:

$$\underline{Z}_E = \frac{U_1}{I_1} = \underline{Z}_{11} - \tilde{\underline{Z}}_{12}\tilde{\underline{Z}}_{22}^{-1}\tilde{\underline{Z}}_{21}. \quad (4.4)$$

Once the input impedance of the multi-port at port 1  $\underline{Z}_E$  is known, the task of determining  $\underline{U}_q$  and  $\underline{Z}_{in}$  results in solving the circuit equations for the circuit shown in figure 4.9. One way of calculating  $\underline{U}_q$  is to summarize the circuit components to  $\underline{Z}_{in}$  as shown in figure 4.10 which results in a simple voltage divider.

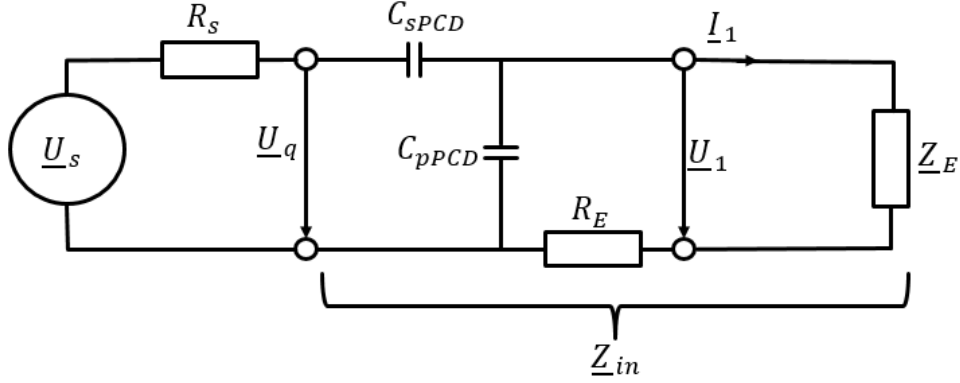


**Figure 4.10:** Circuitry of Poller-0 taking the inductive coupling to Listener-1 and sense into account.

The calculations in MATLAB can be verified by using "EleFAnT2D". Since in "EleFAnT2D" the direct coupling of the FEM problem with the required matching circuits is not implemented, the coil currents  $\underline{I}_1$ ,  $\underline{I}_2$  and  $\underline{I}_3$  have to be computed by solving the multi-port problem shown in figure 4.9. Therefore, the voltages at the coils are known  $\underline{U}_1$ ,  $\underline{U}_2$  and  $\underline{U}_3$ . If the calculations are accurate, the voltage values obtained by the FEM simulation and the solved multi-port equations have to match exactly. The calculations were tested for the following 3 setups:

- Sense coil radius = 25 mm and distance to landing plane = 0 mm
- Sense coil radius = 10 mm and distance to landing plane = 20 mm
- Sense coil radius = 40 mm and distance to landing plane = 40 mm

It was assumed that the sense coil would stay independent of the position of Listener-1 on the landing plane of Poller-0. For Listener-1 the Hmin case was assumed. For the setups listed above perfect approximation was given.

### 4.3 2D examinations

In order to examine the detuning effects of the sense coil to the resonant system of Poller-0 and Listener-1, the magnitude of  $\underline{U}_q$  (see figure 4.10) is investigated. Conveniently, the value of  $\underline{U}_q$  indicates a detuning of the resonant system when it deviates from  $\frac{\underline{U}_s}{2}$ , since Poller-0 is tuned to  $50 \Omega$  at 13.56 MHz without the presence of other coils. Naturally, Listener-1 has a detuning effect on Poller-0. This fact is examined in subsection 4.3.1. In subsection 4.3.2 the effects of the sense coil are compared to the detuning of Listener-1. For all of the following examinations the voltage source delivers  $\underline{U}_s = \frac{5}{\sqrt{2}} V$  in order to comply with [22]. The values of  $\underline{U}_q$  given in the following subsections refer to the root mean square(RMS) value of  $\underline{U}_q$ . For the following examinations the Listener-1 positions in table 4.1 are considered.

### 4.3.1 Case 1- frequency behavior of $U_q$ considering no sense coil

In case 1 only Listener-1 and Poller-0 are present in the operating volume. This makes the calculations described in section 4.2.3 easier since  $[Z]$  becomes a 2 by 2 matrix and only the load of Listener-1 has to be considered. The impedance matrices were extracted from the FEM model, only taking Poller-0 and Listener-1 coils into account. The calculations in MATLAB were carried out analogously to section 4.2.3. For this case, the input impedance  $\underline{Z}_E$  is given by  $\underline{Z}_E = \underline{Z}_{11} - \frac{\underline{Z}_{12}\underline{Z}_{21}}{\underline{Z}_{P ICC} + \underline{Z}_{22}}$ .

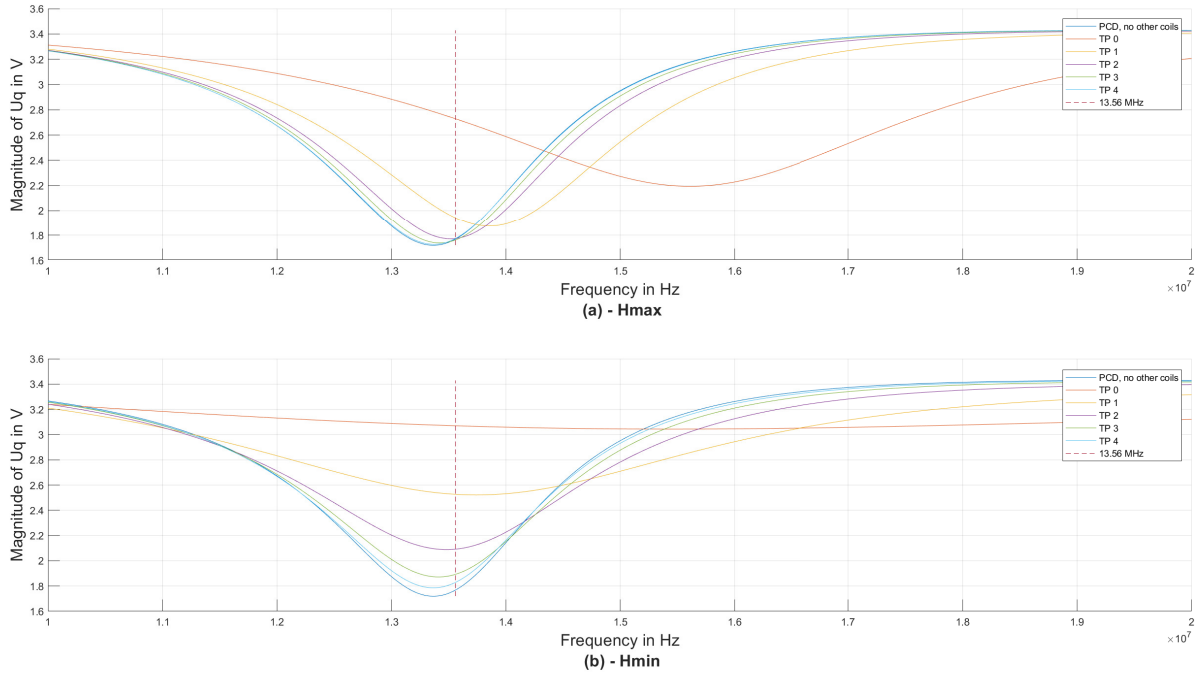
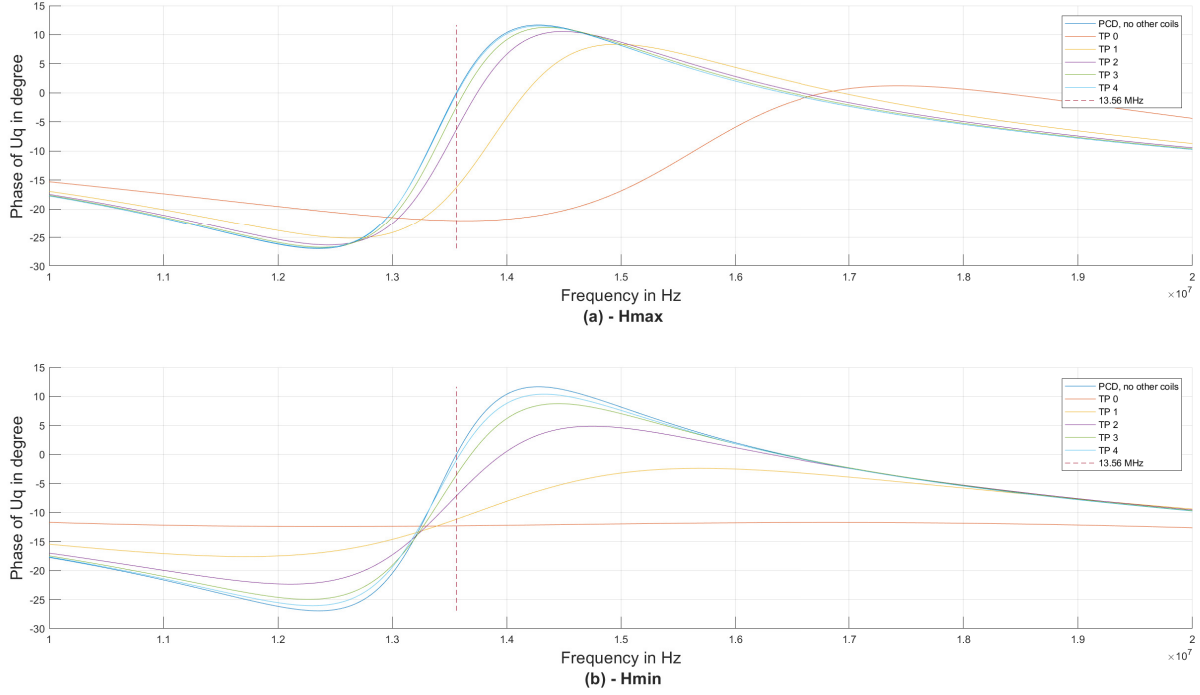


**Figure 4.11:** Case 1 frequency behavior of  $U_q$  considering only Listener-1 in the operating volume. (a) shows the Hmin load case for Listener-1 and (b) Hmax respectively. The operating frequency of 13.56 MHz is indicated with the dashed line. TP 0 to TP 4 refer to the Listener-1 positions considered for the 2D examinations described in table 4.1.

Figure 4.11 shows the magnitude of  $\underline{U}_q$ . As can be seen in figure 4.11, if only the Poller-0 coil is considered then  $\underline{U}_q = \frac{\underline{U}_s}{2}$  at 13.56 MHz. The detuning effect of Listener-1 can be observed by comparing the magnitude of  $U_q$  at the operating frequency. In (a) of figure 4.11 the Hmin case is assumed which results in the value of  $R_{LP ICC} = 450 \Omega$ . In (b) Listener-1 is loaded with Hmax resulting in  $R_{LP ICC} = 50 \Omega$ . As expected, the Hmin case results in a higher detuning effect than the Hmax case. This is apparent when comparing TP 0 from (a) and (b).

The effect of the load of Listener-1 decreases with the distance of Listener-1 to the landing plane, because the inductive coupling of the coils decreases (comparing TP 3 and TP 4 in (a) and (b)).

In essence, the detuning is depended on the distance of Listener-1 to Poller-0 and the load of the listener.



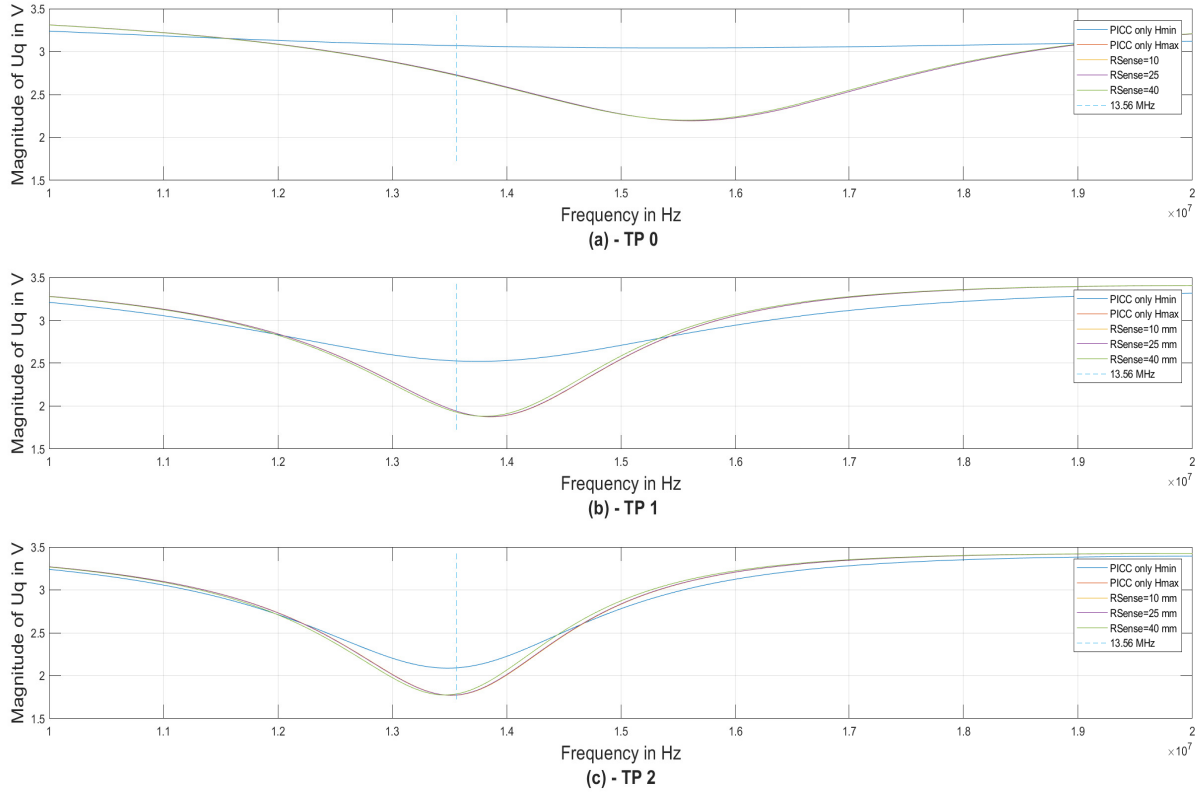
**Figure 4.12:** Case 1 frequency behavior of the phase of  $U_q$ . (a) shows the Hmax load case and (b) the Hmin load case for Listener-1.

Figure 4.12 shows the phase of  $U_q$  for the Hmin case in (a) and for the Hmax case in (b). When comparing (a) and (b) the effect of the load at Listener-1 (in form of  $Z_{LPICC}$ ) decreases as the distance to the landing plane increases.

### 4.3.2 Frequency behavior of $U_q$ - considering sense coil influence

In this subsection the change in the magnitude of  $U_q$  is investigated, considering the influence of a sense coil in the operating volume. The sense coil is terminated with  $Z_{sense}$  as described in section 4.2.3 for case 3 (figure 4.15 and 4.15). Case 2 (figure 4.13 and 4.14) takes the input impedance of the oszillocope into account and neglects the effects of the coaxial cable. The influence of the following 3 sense coils with one turn with radii of 10 mm, 25 mm, 40 mm is considered. For both test cases, the impedance matrix results in a 3 by 3 matrix. Hence, the value of  $U_q$  was obtained as described in section 4.2.3. The results from subsection 4.3.1 are used as reference. The sense coil is assumed to be placed on the landing plane of Poller-0 for all test points. For both test cases the influence of the sense coil is examined assuming the Hmax load case for Listener-1. Hmax was selected as load for Listener-1 due to the fact that it results in a lower influence of Listener-1 on the

resonant system compared to the Hmin case. Hence, the influence of the sense coil can be better observed. For reference also the load case Hmin is shown.



**Figure 4.13:** Case 2 comparing the influence of different sense coil radii to the influence of Listener-1. The frequency behavior of  $U_q$  is shown. As reference the case in which only Listener-1 is present in the operating volume of Poller-0 with Hmin and Hmax is shown. (a) shows the magnitude of  $U_q$  for TP 0, (b) for TP 1 and (c) for TP 2.

Figure 4.13 shows the influence of the sense coil for TP 0 to TP 2. At test points which are close to the landing plane of Poller-0 (such as TP 0 and TP 1), the influence of Listener-1 seems to dominate the influence of the sense coil.

When the distance between the landing plane and Listener-1 increases, the influence of the sense coil on the resonant system increases, since the inductive coupling of Listener-1 to Poller-0 decreases. The sense coil, on the other hand, stays at the landing plane and therefore, the inductive coupling between the sense coil and Poller-0 coil is approximately constant. This effect can be observed by comparing the influence of the sense coil with the radius of 40 mm in figure 4.13 (a) to (b) in figure 4.14.

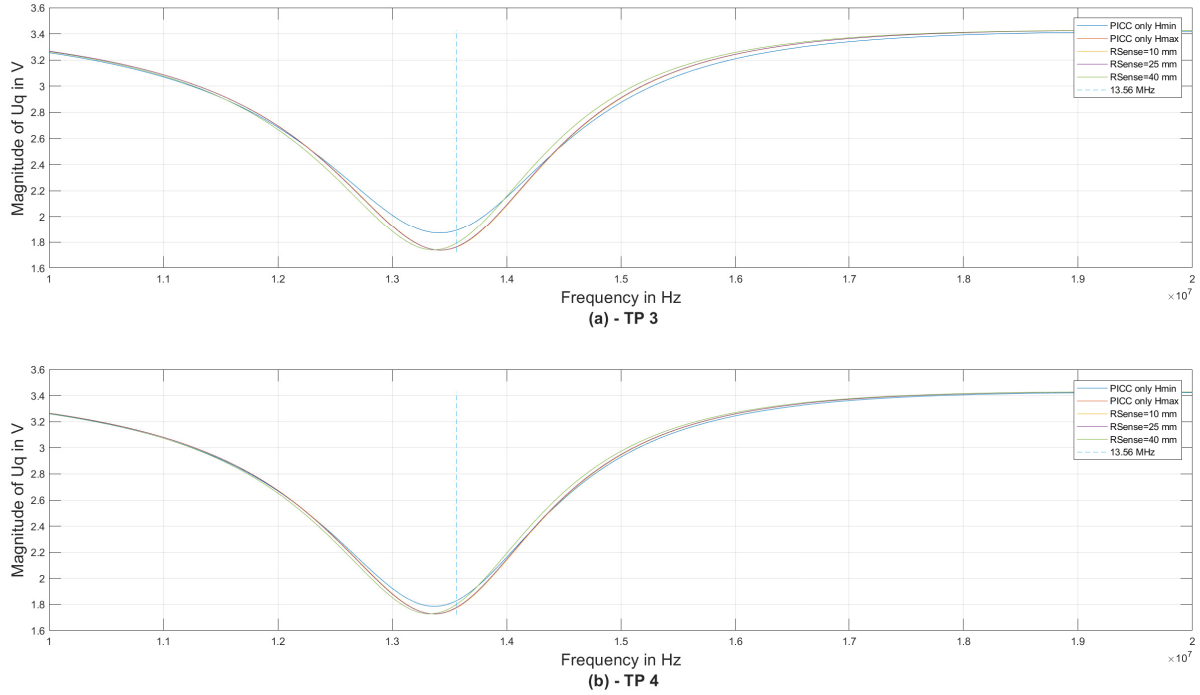


**Figure 4.14:** Case 2 comparing the influence of different sense coils to the influence of Listener-1 in TP 3 to TP 4. As reference the case in which only Listener-1 is present in the operating volume of Poller-0 with Hmin and Hmax is shown. (a) shows the magnitude of  $\underline{U}_q$  for TP 3 and (b) for TP 4.

However, the influence of the sense coil with a radius of 40 mm seems to have less impact on the resonant system compared to the load case of Listener-1, even at TP 4 (see (b) in figure 4.14).

Figures 4.15 and 4.16 show case 3. The sense coil is loaded with  $\underline{Z}_{sense}$  as described in subsection section 4.2.3, taking the input impedance of the oszillocope and the coaxial cable into account. By comparing the frequency behavior of  $U_q$  for the 3 coil radii for TP0 to TP4 (see (a) to (c) in figure 4.15, and (a) to (b) in figure 4.16) the following 2 characteristics can be observed. First, as in case 2 the influence of the sense coil increases with the distance of Listener-1 to the landing plane. Secondly, the sense coils with a radius of 40 mm and 25 mm show a significant influence on the resonant system of Poller-0 and Listener-1. By taking the coaxial cable into account in terms of a loss free cable, the load impedance of the sense coil is decreased. Hence, a higher influence compared to case 2 is expected. However, the effect of the sense coil on the resonant system decreases with the coil radius as can be seen in figure 4.16 in (b). For a coil with 10 mm radius, the influence on the resonant system becomes small despite the lower load impedance.

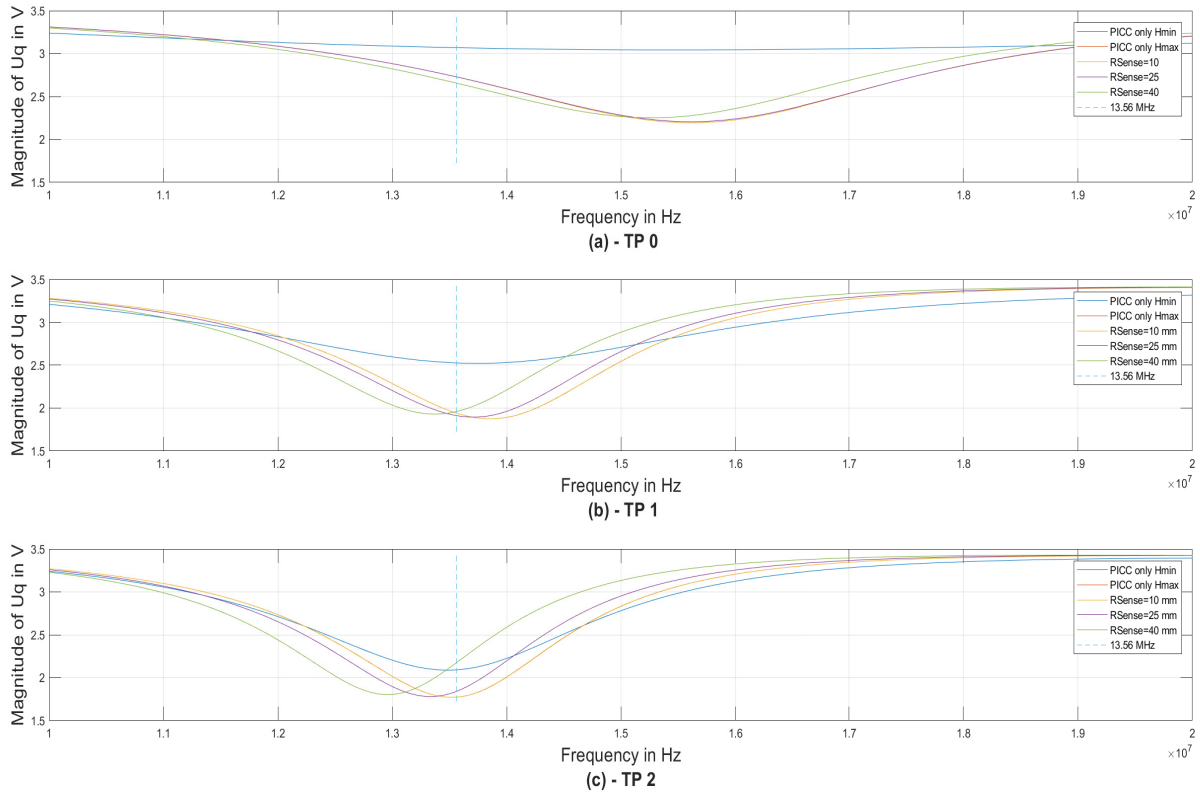


**Figure 4.15:** Case 3 comparing the influence of different sense coil radii to the influence of Listener-1. The frequency behavior of  $U_q$  is shown. As reference the case in which only Listener-1 is present in the operating volume of Poller-0 with Hmin and Hmax is shown. **(a)** shows the magnitude of  $U_q$  for TP 0, **(b)** for TP 1 and **(c)** for TP 2. Due to the small difference between  $R_{\text{sense}} = 10 \text{ mm}$  (orange line) and PICC only Hmax (red line), PICC only Hmax is hidden behind  $R_{\text{sense}} = 10 \text{ mm}$ .

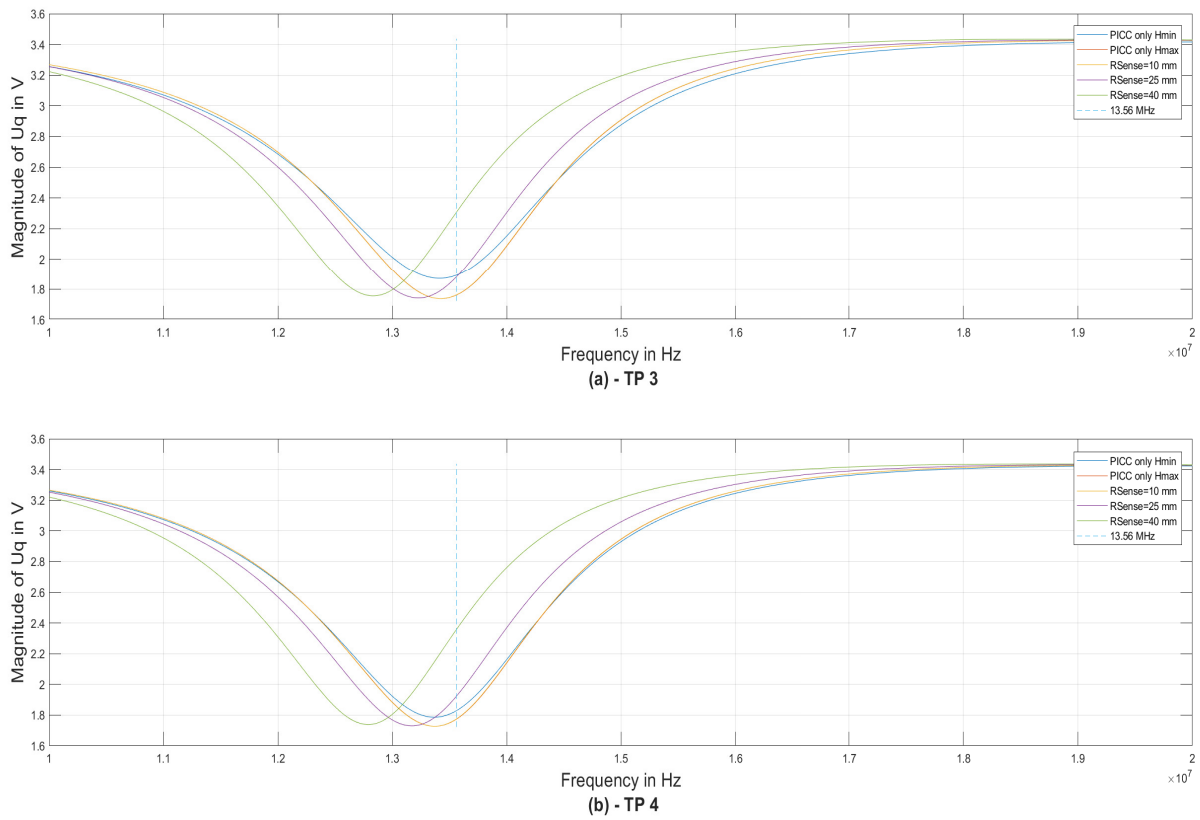


**Figure 4.16:** Case 3 comparing the influence of different sense coils to the influence of Listener-1 in TP 3 to TP 4. As reference the case in which only Listener-1 is present in the operating volume of Poller-0 with Hmin and Hmax is shown. **(a)** shows the magnitude of  $\underline{U}_q$  for TP 3 and **(b)** for TP 4. Due to the small difference between  $R_{\text{sense}} = 10 \text{ mm}$  (orange line) and PICC only Hmax (red line), PICC only Hmax is hidden behind  $R_{\text{sense}} = 10 \text{ mm}$ .

## Chapter 5

# 3D-Optimization

The optimization process relies on a scalar objective function in which the objectives are summarized by means of membership functions as is described in section 5.2. A very naive implementation of the DE strategy was selected for the optimization of the sense coil geometry. For the optimization process a proprietary framework was used.

Therefore, it is required to formulate a cost function in which the forward problem is solved and then accordingly mapped to a scalar quality. For this purpose, the PEEC method is applied in order to create a 3D model of the setup which is then solved resulting in the desired objectives.

### 5.1 Forward Problem - Partial equivalent element circuit method

In order to compute the forward problem a one-dimensional PEEC method is applied. Therefore, the coil geometries and circuitries of Poller-0, Listener-1 and the sense coil have to be modelled accordingly by so called stick-elements. For this purpose, pre-existing models, functions and PEEC solvers are used from the proprietary in-house frame work.

#### 5.1.1 PEEC model of Poller-0

The two main parts of the Poller-0 model are the coil structure and the matching circuit. As a starting point a model from the departments database was modified. The coil geometry can be seen in figure 5.1 in the X-Y plane. The blue dots mark the start and the end points of the stick elements. The parameters that were used in order to model Poller-0 are summarized in table 5.1. The specific resistance  $\rho$  is  $1.786 \cdot 10^{-8} \Omega m$  which corresponds to copper.

The stick elements used in the applied implementation of the PEEC method are cylindrical. Therefore, the rectangular tracks of Poller-0 have to be transformed. The radius of the cylindrical stick elements were chosen based on previous investigations at the institute.

Parameter	Value
number of stick elements per quarter circle	20
number of stick elements for bridges	3
number of stick elements feed line	11
stick element radius	167 $\mu m$

**Table 5.1:** Poller-0 geometrical parameters

These results, were obtained by calculating the losses per unit length applying a 2D FEM simulation of the tracks of Poller-0, taking the skin effect and proximity effects into account.

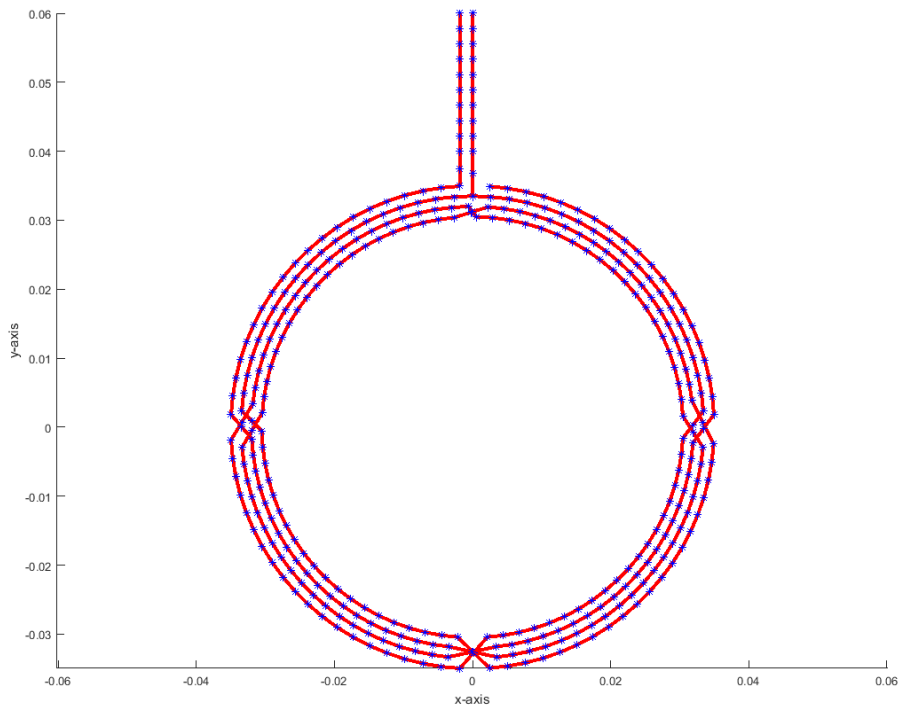


**Figure 5.1:** Poller-0 coil structure of PEEC model

In order to implement the matching circuit and the voltage excitation, the systems of equations resulting from the coil structure is expanded by current- voltage relations, thus introducing appended nodes. The current- voltage relations correspond to the component equations.

The circuitry of Poller-0 which complies with the specifications of the NFC forum is shown in figure 5.2. The green numbers represent the appended nodes for the PEEC implementation. In order to comply with the NFC Forum standard, the applied matching procedure follows the same steps as in section 4.2.1: Using the PEEC geometry and a current excitation, the input impedance of the coil structure of Poller-0 was obtained under the

condition that no other coils are present. Then  $C_{sPCD}$  and  $C_{pPCD}$  were determined such that  $Z_{inPCD} = 50 \Omega$  at operating frequency. The circuit components of figure 5.2 are summarized in table 5.2. The values obtained by the 2D FEM model and the NFC Forum reference range are presented.

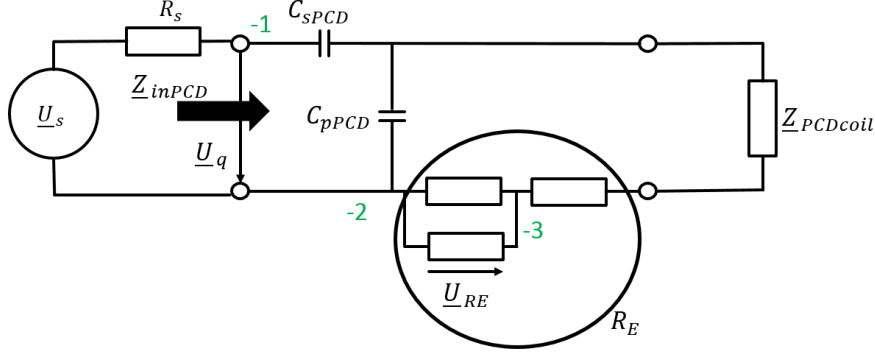


**Figure 5.2:** Matching circuit Poller-0 for PEEC model

Circuit components	Obtained values 2D	NFC Forum reference range	Obtained values 3D
$C_{sPCD}$	74.39 pF	63.6 pF - 72.8 pF	67.8 pF
$C_{pPCD}$	139.93 pF	107.8 pF - 117 pF	128.5 pF
$R_E$	5.2617 $\Omega$		
$Z_{PCDcoil}$	(0.515 + j55.96) $\Omega$	-	(0.482 + j60.92) $\Omega$
$R_s$	50 $\Omega$ ([22] page 5-7)		
$U_s$	5 V <sub>p</sub> at 13.56MHz ([22] page 5-7)		

**Table 5.2:** Obtained and reference values ([1] page 78) for PCD matching circuit.

### 5.1.2 PEEC model of Listener-1

The coil geometry of Listener-1 was modelled according to the NFC Forum specifications, as can be seen in figure 5.3 which shows the X-Y view of the 3D model. Compared to the the track width of Poller-0 (1 mm), the track width of Listener-1 is smaller (0.5 mm), a stick-element radius of 100  $\mu m$  is applied. Again this value is based on results available at the institute, which were obtained using the same process as for the stick element radius of Poller-0, see section 5.1.1.

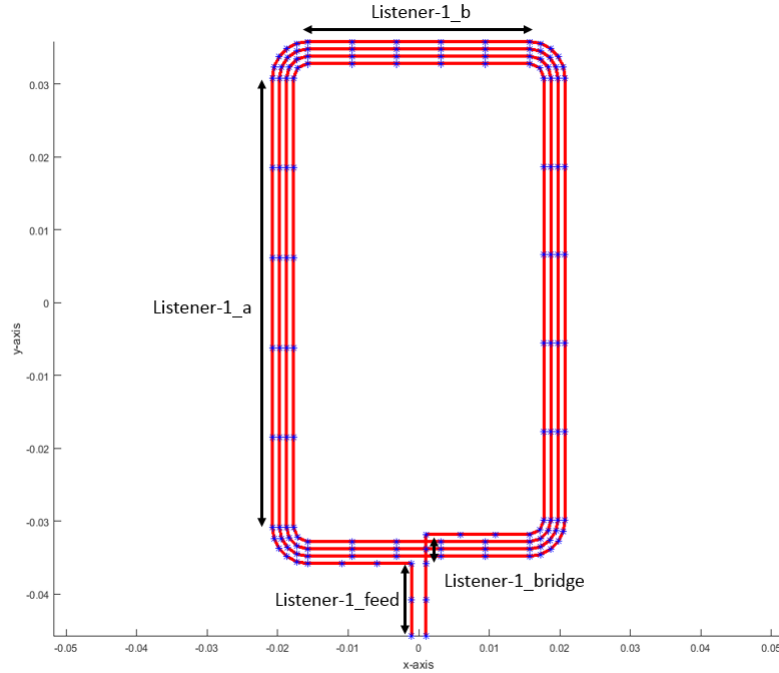


**Figure 5.3:** Listener-1 coil structure. Shows the X-Y view of the 3D model. The blue dots indicate the start and end points of the stick elements.

The discretization of Listener-1 was determined by examining the change of the coil impedance  $\underline{Z}_{P ICC}$  when changing the number of stick elements. The goal is to provide good simulation results by using as few stick elements as possible, since a high number of stick elements results in increased computational effort. The results of this examination are shown in figure 5.4. For this purpose Listener-1 is excited by means of a current source. The number of stick elements applied is then increased until no further significant improvement can be reached by increasing the number of stick elements further. This results in the maximum number of stick elements shown in table 5.3. Figure 5.4 shows the real and imaginary part of  $\underline{Z}_{P ICC}$ , depending on the percentage of the maximum number of stick elements that are applied. The number of stick elements selected for the optimization was chosen in a way that the deviation of the real and imaginary part of  $\underline{Z}_{P ICC}$  is smaller than 1%, compared to the values obtained with the maximum number of stick elements.

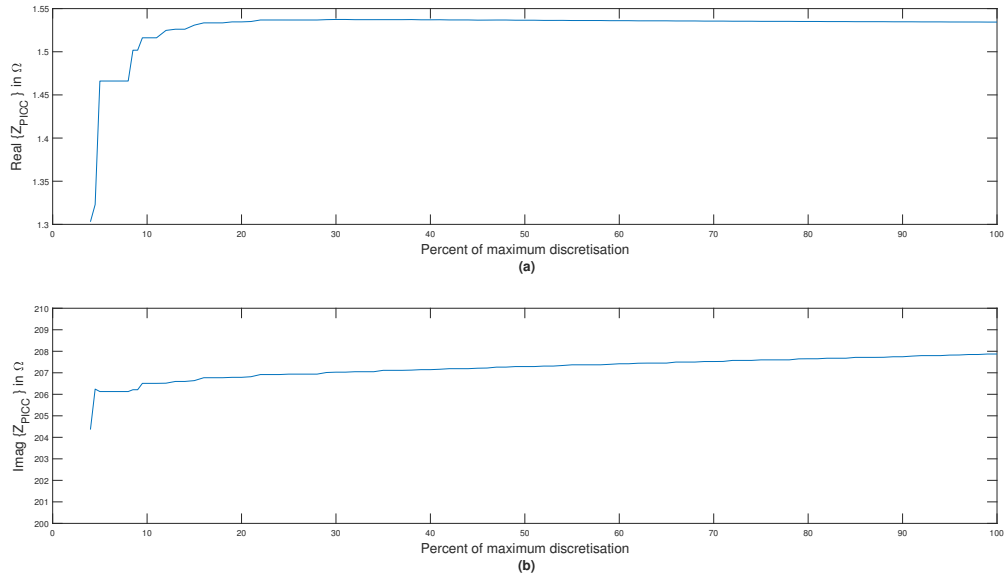


**Figure 5.4:** Change in input impedance of Listener-1 coil, depending on the number of stick elements used. The maximum number of stick elements, shown in table 5.3, are 100 % in (a) and (b). (a) shows the real part and (b) the imaginary part of  $Z_{PICC}$ .

Geometric parameter	Maximum number of stick elements	Number of stick elements applied in optimization
listener-1_a	30	5
listener-1_b	30	5
listener-1_feed	12	2
listener-1_bridge	12	2
listener-1_corner	16	2

**Table 5.3:** Number of stick elements for Listener-1. The geometric parameters refer to the lengths given in figure 5.4. listener-1\_corner refers to the innermost corner of the Listener-1 coil with a radius of 2 mm.

The obtained impedance of  $Z_{PICC3D} = 1.5 \Omega + j\omega 2.40 \mu H$  shows a deviation in the real and imaginary part compared to the obtained listener impedance of the 2D simulation  $Z_{PICC2D} = 1.26 \Omega + j\omega 2.10 \mu H$ . The deviation in the real part is due to the fact that the 2D simulation considers a surface equivalent circular model. Hence, the conductor length is smaller and therefore results in decreased ohmic losses. The deviation in the imaginary part can be explained by the effect of the inner inductance. The PEEC model assumes a constant current density in each stick element, neglecting skin and proximity effects. In order to illustrate this fact, the track width of the 2D Listener-1 model is reduced and the resulting values of the obtained impedances are summarized in table 5.4. As one can see in table 5.4, the inductivity increases as the track width decreases, whereas the coil resistance  $R_{PICCcoil}$  increase due to the decrease in the cross-sectional area. By decreasing

the track width the inner inductance is increased. Hence, the value obtained for the coil inductance  $L_{P\text{IC}C\text{coil}}$  for a track width of  $50 \mu\text{m}$  shows already only a small deviation from the obtained coil inductance of the PEEC model. In conclusion, the PEEC model overestimates the inductance of the coil structures due to the assumption of a constant current density in each stick element.

Track width in $\mu\text{m}$	$R_{P\text{IC}C\text{coil}}$ in $\Omega$	$L_{P\text{IC}C\text{coil}}$ in $\mu\text{H}$
500	1.5	2.10
100	4.4	2.30
50	7.7	2.36

**Table 5.4:** Impedances of the 2D Listener-1 model with varying track width. The track width is reduced in a way that the inner side of the track complies with the standard.

In order to comply with the NFC Forum requirements for Listener-1 circuitry, the model described in subsection 4.2.2 is also used for the PEEC model of Listener-1. The circuitry is shown in figure 4.8 in section 4.2.2. The matching capacitance  $C_{pP\text{IC}C}$  was determined by calculating the input impedance of the coil structure of Listener-1  $Z_{P\text{IC}C\text{coil}}$ , as described in subsection 4.2.2. In contrast to the 2D model, in the PEEC model capacitive effects are considered in  $Z_{P\text{IC}C\text{coil}}$ . Then  $C_{pP\text{IC}C}$  was chosen so that  $\text{Im}\{Z_{inP\text{IC}C}\} = 0$  (compare with figure 4.8). By applying this process, the matching capacitance of Listener-1 was determined to be  $C_{pP\text{IC}C} = 57.5 \text{ pF}$ . For the optimization process it is assumed that Listener-1 is loaded with Hmin -  $R_{LP\text{IC}C} = 450 \Omega$ .

### 5.1.3 Testing compatibility with NFC Forum standard

In order to test the compliance with the NFC Forum requirements, step 2 and step 3 of the "NFC Forum Reference Equipment Verification Tests" ([22] page 5-8) for the PEEC model of Poller-0 and Listener-1 were conducted. Here, the magnitude of the voltage  $\underline{U}_{RE}$ , (seen in figure 5.2), is measured. The voltage excitation which is used in the measurement setup described in [22] requires peak values of  $U_s = 5 \text{ V}$  at 13.56 MHz. In the test specification the signal generator is connected to a directional coupler which is connected with both outputs to channels 1 and 2 of the oscilloscope both with an input impedance of  $50 \Omega$ . In this configuration the signal generator is adjusted such that a peak to peak voltage of  $5 \text{ V}$  is measured at the oscilloscope for those output that is later used to supply the poller(channel 2). The voltage value measured with channel 1 is then used as a reference value  $V_{c\text{-ref}}$ .

In step 2 the tuned and matched Poller-0 is connected to the signal generator. The signal generator is then adjusted such that the reference value  $V_{c\text{-ref}}$  is reached. Then the magnitude of  $\underline{U}_{RE}$  is measured.

In Step 3 Listener-1 is placed above Poller-0 in 5 mm distance in z direction. The loads  $820 \Omega$  and  $82 \Omega$  are considered for the listener ([22] page 5-8). The load values refer to the value of  $R_Q$  in figure 4.7, which in the present PEEC model corresponds to the Hmin and Hmax load cases respectively. Before measuring  $\underline{U}_{RE}$  for the Hmin and Hmax case the signal generator is adjusted such that  $V_{c\text{-ref}}$  is reached.

Due to the unknown behavior of the directional coupler and the presence of coaxial cable with losses, the following approach was chosen to approximate the behavior of the test procedure using the PEEC model. Starting with step two, considering only Poller-0 with no other coils present,  $\underline{U}_s$  (see figure 5.2) was selected so that the the magnitude of  $\underline{U}_{RE}$  meets the test criteria. The resulting voltage  $\underline{U}_q = 4.56 V_{pp}$  is then further used as reference for the listener tests in step 3. For step 3 the voltage supply  $\underline{U}_s$  is adjusted such that  $\underline{U}_q = 4.56 V_{pp}$  is reached. The obtained values are summarized in table 5.5.

Test case	NFC Forum reference range in mV	$U_{RE}$ in mV	$U_s$ in V
Poller-0, no other coils present	234.97-244.56	243.21	3.22
Listener-1 Hmin load case	75.91-83.91	70.94	2.11
Listener-1 Hmax load case	161.64-175.10	159.62	2.66

**Table 5.5:** Summary of voltage values of NFC Forum Reference Equipment Verification Tests. The reference values are taken from [22] appendix A. The voltages shown in this table refer to RMS values. No reference potential is taken into account.

Comparing the voltage values of the PEEC model with the NFC Forum reference range in table 5.5, one can see that the PEEC model produces slightly lower voltage values for the listener test than the values given [22] in appendix A (reference range). This could be due to the unknown behavior of the directional coupler and the fact that the no load sense coil of Listener-1 is neglected. For the optimization process  $U_s = 3.22 V_{RMS}$  is applied.

Test case	NFC Forum reference range in mV	$U_{RE}$ in mV	$U_s$ in V
Poller-0, no other coils present	234.97-244.56	243.06	3.22
Listener-1 Hmin load case	75.91-83.91	72.704	2.12
Listener-1 Hmax load case	161.64-175.10	167.98	2.76

**Table 5.6:** Summary of voltage values of NFC Forum Reference Equipment Verification Tests with asymmetrical voltage supply. The reference values are taken from [22] appendix A. The voltages shown in this table refer to RMS values.

For optimization process 3 the PEEC model is excited by means of an asymmetrical voltage supply. Therefore, the NFC-Forum Reference Equipment Verification Tests were performed for this case as well. The results are shown in table 5.6. Noticeably, the Hmax test case is now within the reference range whereas the result of the Hmin test case is only slightly improved.

#### 5.1.4 PEEC model of sense coil

The stochastic optimization process requires the computation of a large variety of sense coil geometries. Therefore, a function that is based on certain parameters which provide the desired variety of coil geometries is necessary. For this purpose a prior student's work was modified and extended. The resulting coil structure is shown for an exemplary geometry in figure 5.7.

The sense coil geometric parameters in table 5.8 are determined during the optimization process. The parameter space consists of the following parameters:

- $A_{sense}$
- $kx$
- $curvature$
- $b_{forbidden}$

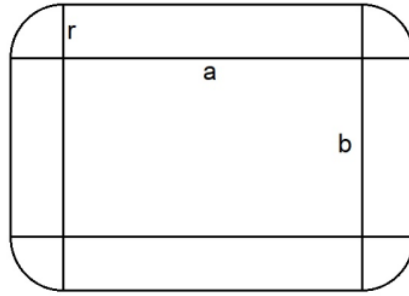


**Figure 5.5:** General coil geometry ([24] page 13).

$A_{sense}$  describes the surface area of the coil geometry, not counting the contribution of the two feed lines, in  $m^2$ .  $kx$  sets the aspect ratio between  $a$  and  $b$  (see figure 5.5) by  $kx = \frac{a}{a+b}$ . The parameter  $curvature$  defines how much of the surface area  $A_{sense}$  is used for the quarter-circle parts and how much is used for the straight elements  $a$  and  $b$ . Hence, at a  $curvature$  of 1 the coil geometry becomes a full circle, and for  $curvature = 0$  the coil geometry results in a rectangular geometry ([24] page 12-14).  $b_{forbidden}$  adjusts the number of turns depending on the surface area  $A_{sense}$  and  $kx$  and the  $curvature$ . It defines a percentage of the lengths  $x_{max}$  or  $y_{max}$  (see figure 5.6) whichever is shorter. The  $length_f$  is determined by  $b_{forbidden}$  times  $x_{max}$  or  $y_{max}$  plus 1  $mm$  to grantee a track distance ( $d_{turn}$ ) of at least 1  $mm$ , even for the innermost turn. The number of turns is then determined in such a way that in  $length_f$  no tracks are present. In figure 5.6  $length_f$  is shown for a rectangular geometry for which  $y_{max} < x_{max}$ .

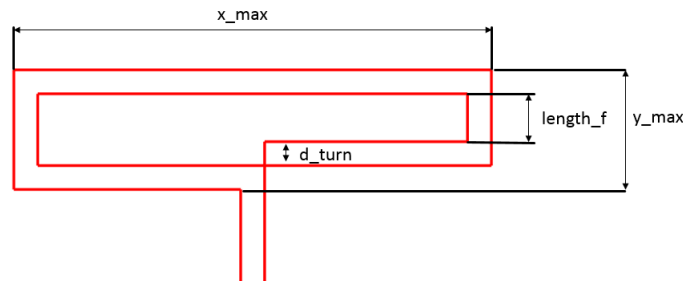


**Figure 5.6:** Example for the number of turns determination.

In order to keep  $d_{turn}$  constant, the coil structure is build up by 3 different methods

with their respective application criteria which are summarized in table 5.7 . For coil geometries with more than one turn either the radius  $r$  or the segment  $b$  are reduced in order to start the next turn. If the *segment* is smaller than  $d\_turn$  then the bottom right hand quarter circle is build up as an ellipse resulting in 3 coil structure creation methods. The coil structure is build up from the outermost turn to the innermost turn and the creation method is switched accordingly. This is the case if a coil starts with method 2 and is then switched to method 1, due to the fact that the radius becomes smaller than  $d\_turn$ .

	Application criterion	Method for coil structure creation method
Method 1	$r \leq d\_turn$	r: constant and segment length: reduced
Method 2	$r > d\_turn$ and $segment > d\_turn$	r: constant and segment length: reduced
Method 3	$segment \leq d\_turn$	Ellipse case

**Table 5.7:** Overview coil structure creation method ([24] page 8. ). *segment* refers to the straight segments of  $a$  and  $b$ .

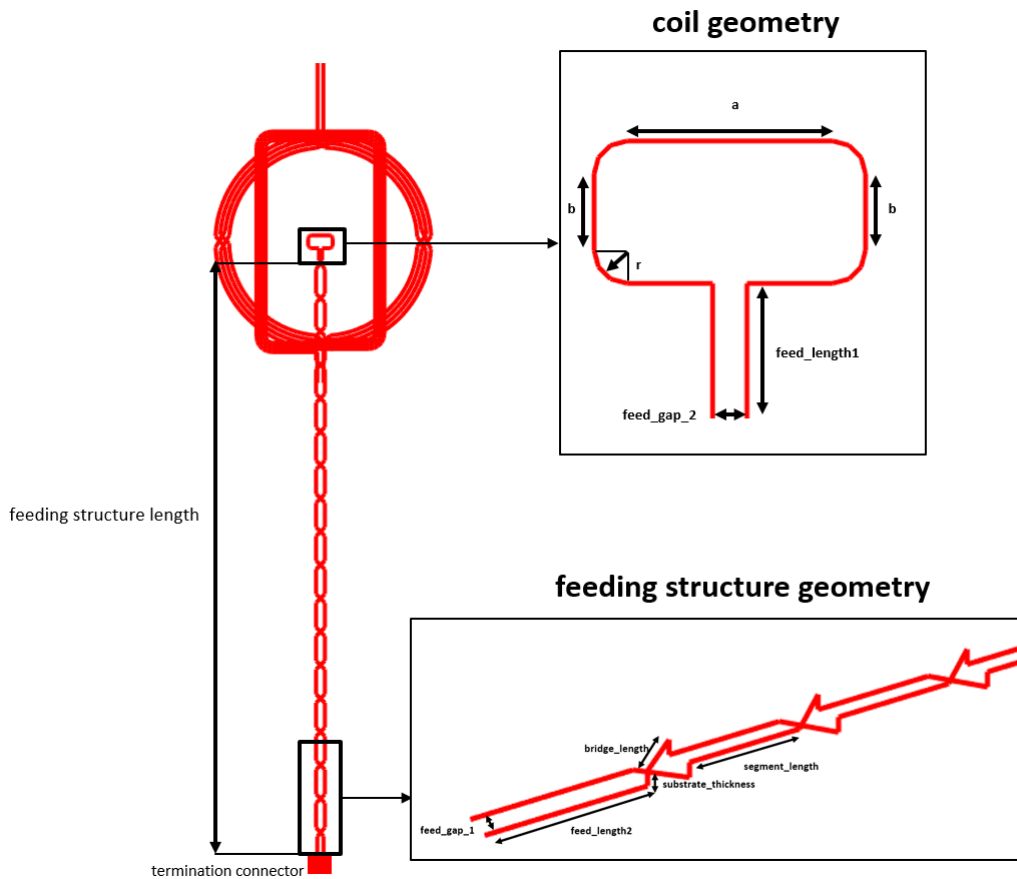


**Figure 5.7:** Exemplary sense coil structure, which consist of the coil geometry and the feeding geometry structure. For simplicity the exemplary coil shown is the best solution obtained by optimization process 1.

The feeding structure was taken from the 8 shaped coil specifications of the NFC Forum ([1] page 98). During the optimization process, the feeding structure geometry is not subject to changes, only the coil geometry itself is optimized. As can be seen in figure 5.7, at the end of the feeding structure there shall be a termination connector. The termination connector is not considered in the PEEC model. The feeding structure length plus  $feed\_length1$  equals a distance of 200  $mm$  and its geometry is displayed in figure 5.7 at the bottom right hand side. Throughout the feeding structure the dimensions  $bridge\_length$  and  $substrate\_thickness$  are constant. The feed gap width was selected with  $feed\_gap\_2 = 1\ mm$  and  $feed\_gap\_1 = 2\ mm$  to allow for an easy connection with the termination connector.

The geometry of the coil consists of four circular segments with the radius  $r$ , connected by straight segments  $a$  and  $b$ , as can be seen in figure 5.13 in the top right hand corner. The distance between the tracks of the coil structure is assumed with 1  $mm$  and is not changed during the optimization process. The values of the geometric parameters seen in figure 5.7 are summarized in table 5.8.

Geometric dimension	Value in mm	number of stick elements applied
$a$	variable	10
$b$	variable	10
$r$	variable	6
number of turns	variable	-
$substrate\_thickness$	0.4	1
$feed\_gap\_1$	2	-
$feed\_gap\_2$	1	-
$feed\_length1$	4	4
$feed\_length2$	9.1	1
$bridge\_length$	4	1
$segment\_length$	8	2
$track\_width$	0.5	-

**Table 5.8:** Summary of geometric parameters for the PEEC model of the sense coil. The  $track\_width$  corresponds to a stick element radius of 100  $\mu m$ .  $a$ ,  $b$ ,  $r$  and number of turns are displayed as variable, since they are subject to change during the optimization process. The number of stick elements for  $r$  refers to the discretization of each circular segment. The displayed number for  $a$ ,  $b$  and  $r$  refer to the maximum number stick elements permitted in the geometric dimension.

In table 5.8 the applied number of stick elements per subsection is shown too. Since, the feeding structure of the sense coil is not subject to changes during the optimization process the number of stick elements is constant.

The discretization of the coil geometry was applied with the following considerations. First, it is necessary to ensure that the stick element length is longer than the stick element radius (100  $\mu m$ ) in order to avoid numerical problems. Secondly, the computational effort should be kept as low as possible. Therefore, the maximum number of stick elements for  $a$ ,  $b$  and  $r$  is applied as shown in table 5.8. Depending on the geometry, these maximum numbers are then reduced as such: For coil geometries which are bigger than 100  $mm^2$  the number

of stick elements in each geometric dimension is reduced so that the stick element length is bigger than  $1\text{ mm}$ , and for geometries smaller than  $100\text{ mm}^2$  is bigger than  $0.5\text{ mm}$ .

Due to the fact that stick element length shorter than ( $100\text{ }\mu\text{m}$ ) are not permitted the following cases occur. If the quarter circle becomes too small, then the circular part of the geometry is neglected and a rectangular coil is created taking into account the neglected radius  $r$ . If  $a$  or  $b$  are smaller than the stick element radius, then the straight element is neglected in the coil geometry as shown in figure 5.8. In such a case the last stick element of the corresponding quarter circle is extended by the neglected length. For example if  $b$  becomes too small, the top right hand corner and the bottom left hand corner circles end exactly where where the stick element of  $b$  ended. In figure 5.8 shows this for the case that  $a$  and  $b$  are neglected.

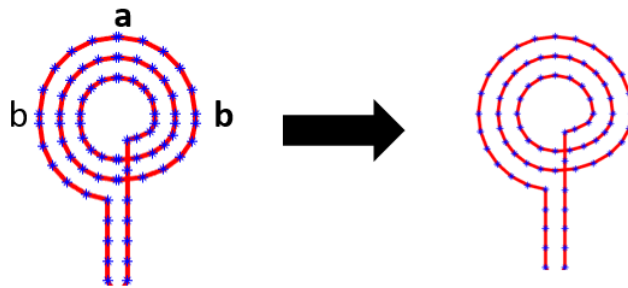


**Figure 5.8:** Discretization example of coil geometry 1. Shows how the coil geometry changes when neglecting the lengths  $a$  and  $b$ .

The same logic is applied if the straight segments to and from the feed line become smaller than the element radius. In figure 5.9 these two stick elements are highlighted with circles.

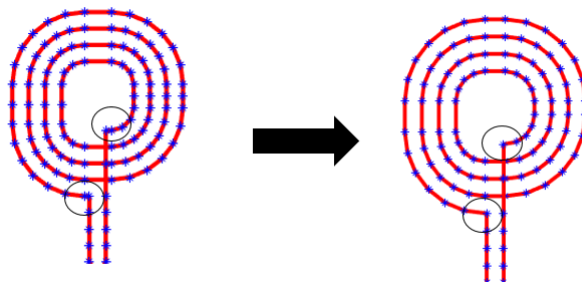


**Figure 5.9:** Discretization example of coil geometry 2. Shows how the coil geometry changes when neglecting the lengths straight segments from and to the feed line. The geometries shown are not identical. For the geometry on the right, the curvature was increased compared to the curvature on the left.

The track properties were taken from the track properties of Listener 1 of the NFC-Forum which specify that the "outer Layers (1 oz Cu weight): 18 microns (before plating) and

35 microns (after plating)" ([1] page 95) and has a track width of 0.5 mm ([1] page 91). Since the applied PEEC implementation requires the conductors to be modelled in terms of cylindrical stick elements, the resulting stick element radius is  $100 \mu m$  (see also section 5.1.2).

The load impedance of the sense coil is implemented, as described in section 3.4, which results in one additional appended node.

## 5.2 Formulation of the Optimization- Problem

With the PEEC models of Poller-0, Listener-1 and sense coil as described in subsections 5.1, 5.1.2 and 5.1.4 the forward problem of the optimization process can be formulated. The objectives were chosen under the following considerations.

The sense coil shall have as small as possible influence on the resonant system consisting of Poller-0 and Listener-1, by generating in the "worst" listener position in the EMVCo volume a voltage of at least  $10 mV$  and  $15 mV$  for the oscilloscope, as described in section 3.4. As a result, one objective naturally has to be the voltage provided by the sense coil  $U_{sense}$ .

The second objective has to provide a measurement for the influence of the sense coil on the resonant system. For this purpose,  $\underline{U}_q$  (see figure 5.2) is considered. Therefore, reference values  $\underline{U}_{q_{ref}}$  were calculated for each listener position, prior to the optimization process in which only Poller-0 and Listener-1 are taken into account. Then  $U_{q_{diff}}$  is calculated as  $U_{q_{diff}} = |\underline{U}_{q_{ref}} - \underline{U}_{q_{sense}}|$ , whereas  $\underline{U}_{q_{sense}}$  is the value of  $U_q$  taking the sense coil influence into account.

Due to the fact that all test points in the EMVCo operating volume have to be considered, the strategy for both objectives is to evaluate each listener position in order to find the "worst" value in the EMVCo operating volume. This results in two objectives which are returned to the optimization framework:

- $U_{sense\_min} = \min(U_{sense})$  , for all EMVCo test points
- $U_{pcd\_max} = \max(U_{q_{diff}})$ , for all EMVCo test points

The DE framework requires the objective function to return a scalar quality. Therefore, the two objectives are quantified by using membership functions in terms of fuzzy functions. The output of the fuzzy functions (quality contribution of each objective) are then added to obtain the desired scalar quality. The fuzzy functions map the values of the objectives  $U_{pcd\_max}$  and  $U_{q_{diff}}$  to values between 0 and 1. Due to the fact that the sense coil is required to provide at least  $10 mV$  or  $15 mV$  the choose fuzzy function for  $U_{sense\_min}$  has a very step characteristic. This is due to the fact that it is only of interest that the voltage requirement is met. Coil geometries which produce higher  $U_{sense\_min}$  are preferable, however it is unacceptable to miss this requirement.

The fuzzy functions, in the applied implementation, are defined by the objective values which result in a quality contribution of 0.9 and 0.1. The resulting scalar quality is min-

imized during the optimization process. Hence, a high quality represents a non desirable solution, whereas low qualities indicate "good" solutions of the optimization process.

In order to avoid numerical difficulties, the distance in Z-direction between the coils is assumed with the conductor radius of the stick elements. The resulting distances are shown in figure 5.10.

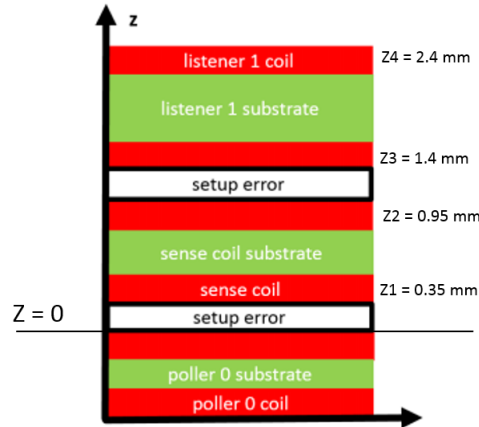


**Figure 5.10:** Schematic coil positioning in Z-direction for 3D coil models. Red indicates a track, green substrates and white the assumed setup error see subsection 4.1.3. Z1 to Z4 show the track to the landing plane at  $Z = 0$ . The bridges of sense and listener coil are indicated by the tacks at Z2 and Z3.

### 5.3 Optimization results

Using the formulation of the optimization problem described in section 5.2, the results of two optimization processes are presented. In subsection 5.3.1 sense coil is required to deliver  $U_{sense} > 10 \text{ mV}$ , whereas in section 5.3.1  $U_{sense}$  is required to surpass  $15 \text{ mV}$ . For both optimization processes the Hmin load case for Listener-1 was assumed. In order to decrease the computational effort the test points in the EMVCo volume have been reduced to the relevant ones. This was done by performing two optimization runs using the entire EMVCo volume and logging the positions at which the the minima and maxima values have been obtained. The first optimization run was performed with 100 iterations and 20 individuals and the second one with 10 iterations and 50 individuals. The obtained test positions within the EMVCo volume are summarized in table 5.9.

The objectives shown in the optimization processes had to be recalculated after the optimization process. Unfortunately, due to a logging error in the used framework (which could not be localised), the objectives values which were logged during the optimization process did not correspond to the resulting quality. Nevertheless, the recalculations have shown that the quality values obtained during the optimization process correlate to the recalculated values of the objectives. Due to the fact that the DE algorithm relies on the value of the quality, it is supposed that the logging error does not influence the optimization process and hence with the convergence behavior of the parameters.

Test position	x in mm	y in mm	z in mm
TP 1	0	0	2.4
TP 2	15	0	2.4
TP 3	-15	0	2.4
TP 4	0	15	2.4
TP 5	15	0	42.4
TP 6	-15	0	42.4

**Table 5.9:** EMVCo test points for optimization. The table shows Listener-1 positions which were taken into account during the optimization.

### 5.3.1 Optimization process 1

In the optimization process 1 the box constraints for the parameters are summarized in table 5.10. A population of 20 individuals is selected, due to the relatively small parameter space. As stopping criteria the maximum number of iterations of 50 was chosen. The values for the best solution, which resulted from the optimization process, are shown in table 5.10.

Parameter	Min value - max value	Obtained values for best coil geometry
$A_{sense}$	11 – 1000 mm <sup>2</sup>	32.22 mm <sup>2</sup>
$k_x$	0.2 – 0.8	0.73
<i>curvature</i>	0 – 1	0.09
$b_{forbidden}$	0.1 – 1	0.77

**Table 5.10:** Optimization process 1 parameter space and best obtained solution

Objective	Fuzzy function value of 10%	Fuzzy function value of 90%
$U_{sense\_min}$	11 mV	10 mV
$U_{pcd\_max}$	0.01 mV	8 mV

**Table 5.11:** Optimization process 1 values for fuzzy functions

Since, the aim of the objective  $U_{sense\_min}$  is to ensure that the resulting sense coil geometry produces  $U_{sense\_min} > 10$  mV, the corresponding fuzzy function was chosen to have a very steep increase in quality contribution, between 11 mV to 10 mV. Hence, a sense coil producing  $U_{sense\_min} > 11$  mV, is valued with a "good" quality. However, if the sense coil provides  $U_{sense\_min} < 11$  the solution is penalized with a "bad" quality. The aim of  $U_{pcd\_max}$  is to become as small as possible. Hence, the value for 10% was chosen very low. The value for 90 % was selected during sample runs such that the quality in the process, shows a descent decline in quality. If the value is chosen too low the gradient might not be found during the optimization process. The values used for the fuzzy functions are shown in table 5.11.

Figure 5.11 shows the convergence behavior of the optimization parameters and the corresponding number of turns for all 10 runs conducted. For each iteration the parameters which delivered the best quality are shown.

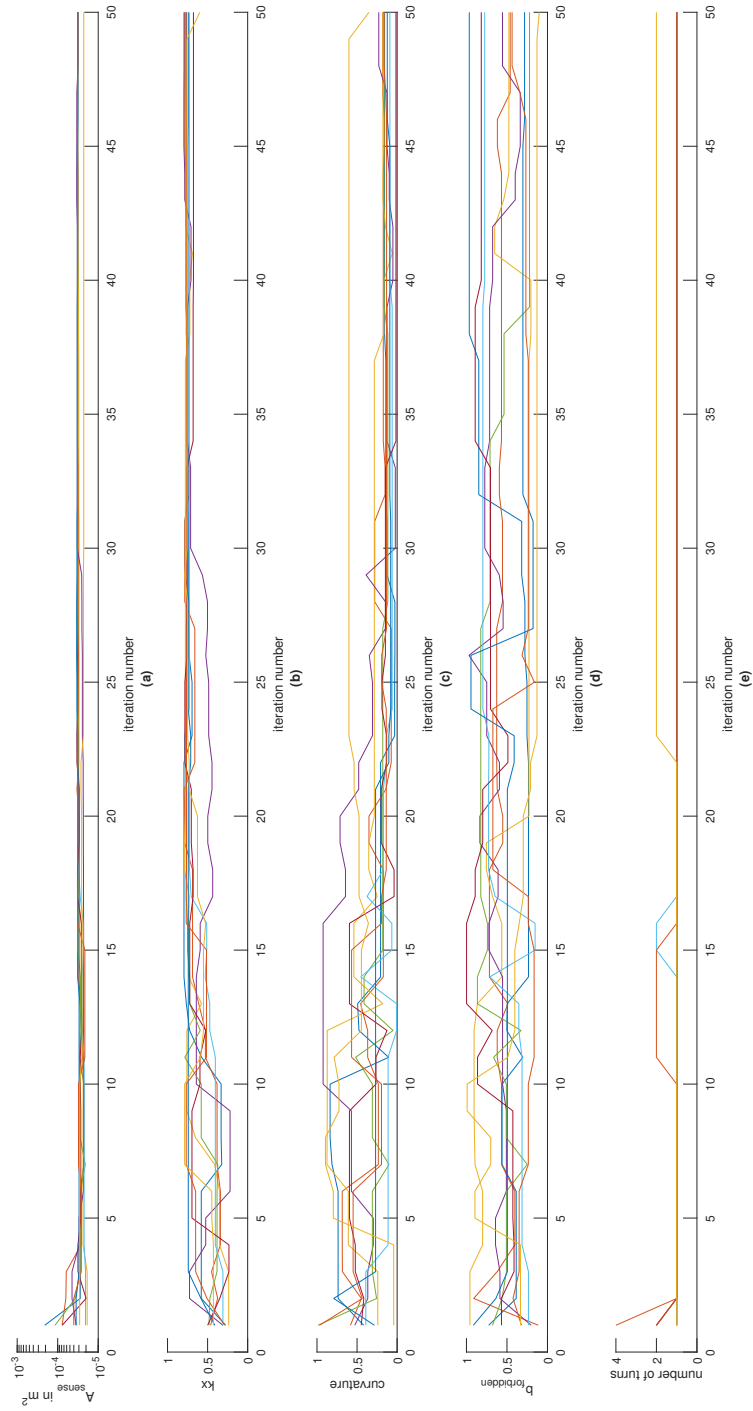


**Figure 5.11:** Optimization process 1 convergence behavior of the geometry parameters and the return value "number of turns".

As can be seen in figure 5.11 in **(a)**, the surface area of the sense coil  $A_{sense}$  trends very fast towards the lower boundary of the parameter space. The convergence behavior of  $b_{forbidden}$  shown in **(d)** in figure 5.11 seems inconclusive. The parameter  $b_{forbidden}$  is used to describe the number of turns permitted for a given sense coil geometry, therefore it is depending on  $A_{sense}$ ,  $curvature$  and  $kx$ . For small surface area sense coils,  $b_{forbidden}$  is therefore required to become small to allow for more than one turn. As a result,  $b_{forbidden}$  is permitted a wide range of values which results in a one turn as can be seen in figure 5.11 by comparing **(d)** and **(e)** for iterations  $> 30$ . Therefore, the numbers of turns is displayed in **(e)**, which clearly shows a fast convergence behavior towards a one turn coil. One run however resulted in a two turn coil which produces a worse quality then the one turn solutions. Also  $kx$  **(b)** and  $curvature$  **(c)** show very clear convergence behavior.

Figure 5.12 shows the convergence behavior of the objectives  $U_{sense\_min}$  in **(a)**,  $U_{pcd\_max}$  in **(b)** and the resulting quality in **(c)**. As in figure 5.11, the values for the best quality achieved in each iteration are displayed for all 10 runs. As can be seen in **(c)**, the quality shows clear convergence behavior.

As can be seen in figure 5.12 the quality of the 10 runs tends towards a low value but not zero. The reason for this is the choice of the 10% value for  $U_{pcd\_max} = max(U_{q\_diff})$  in table 5.11. Therefore, it is impossible for a coil that produces more than 10 mV of voltage to obtain a quality of zero.

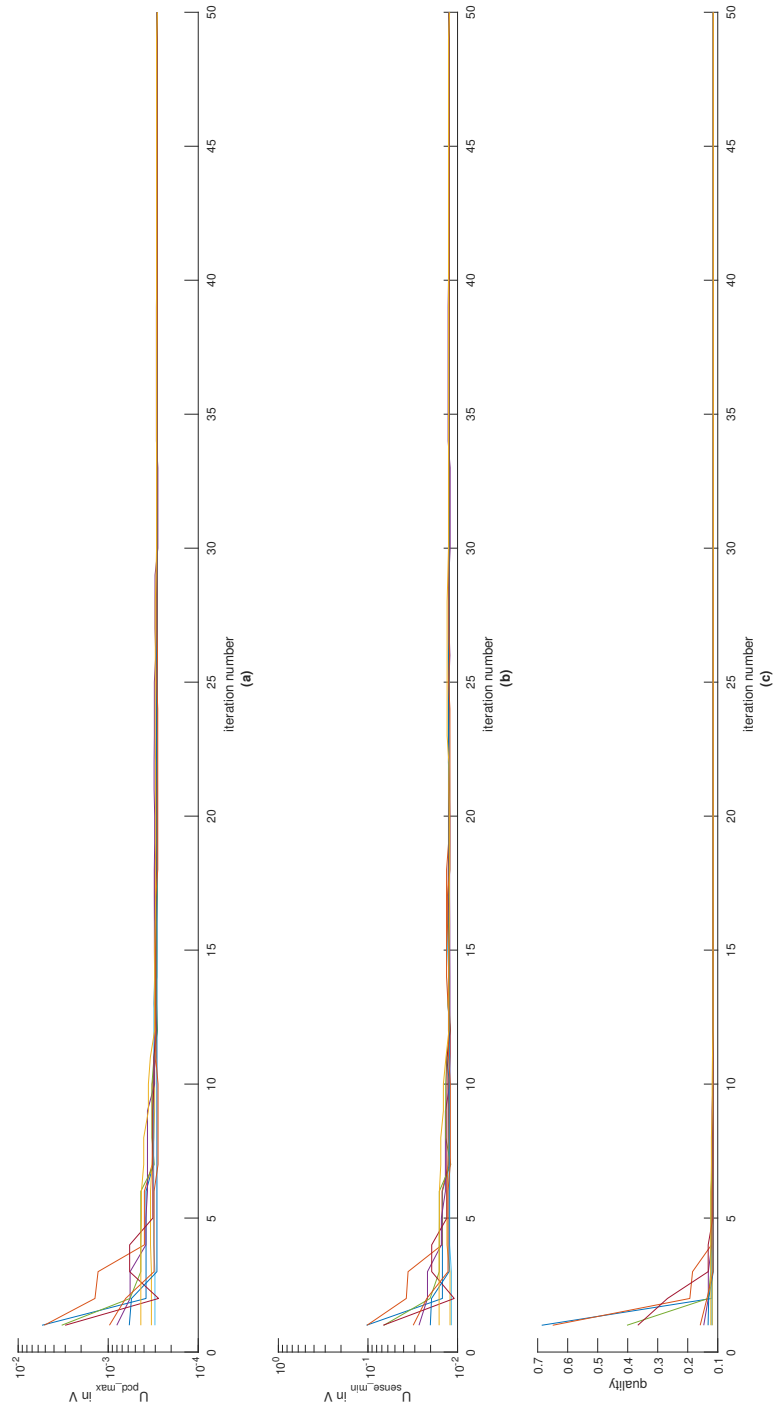
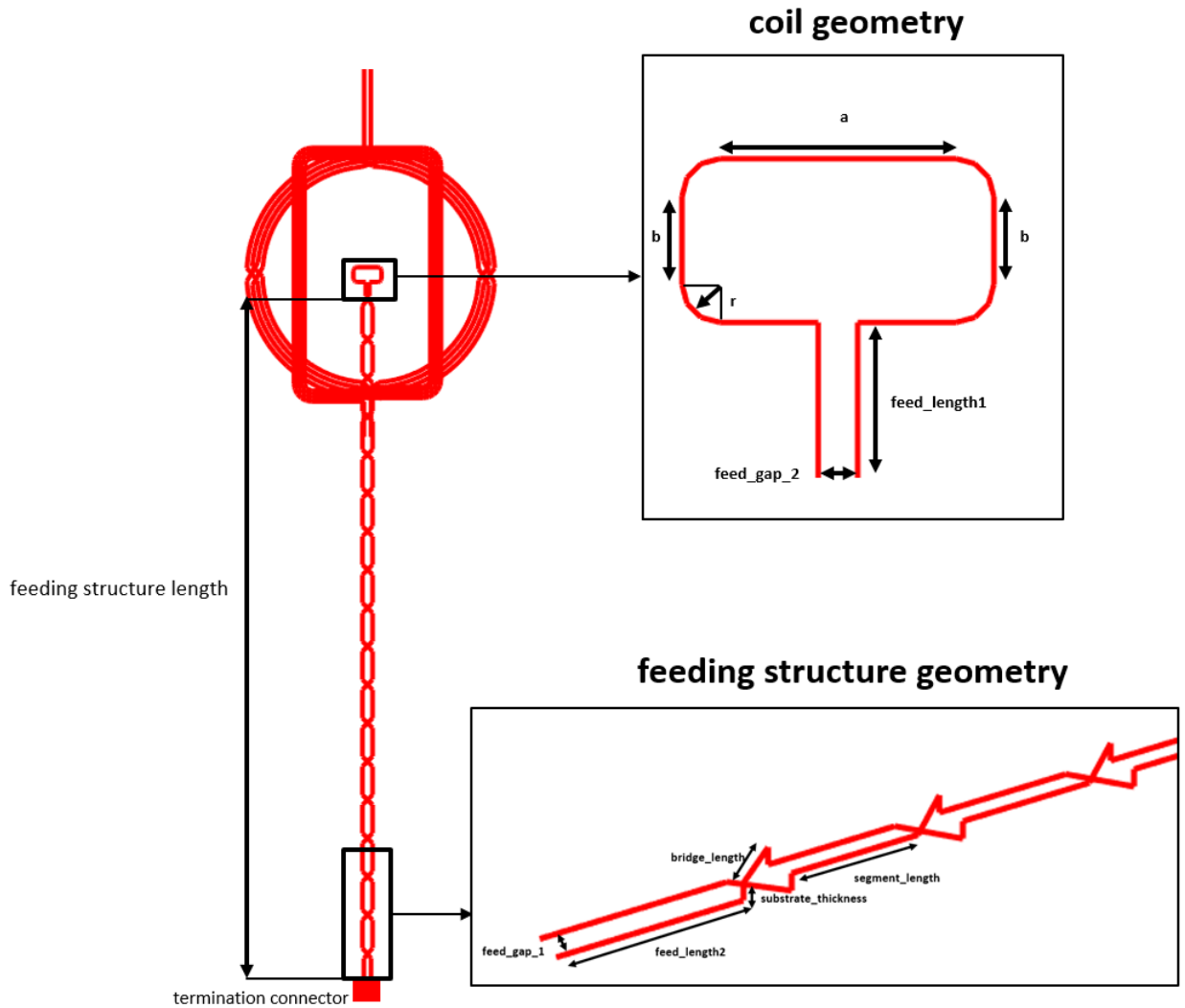


Figure 5.12: Optimization process 1 convergence behavior of objectives and quality.

In figure 5.13 the coil geometry showing the best quality during the optimization process is displayed. In table 5.12 the corresponding geometric dimensions are summarized. The geometry of the feeding structure is described in section 5.1.4. The coil geometry displayed in figure 5.13 results in  $U_{sense\_min} = 12.56 \text{ mV}$  and  $U_{pcd\_max} = 0.286 \text{ mV}$ .



**Figure 5.13:** Optimization process 1 sense coil geometry for best solution

Geometric dimension	Value
$a$	5.994 mm
$b$	2.244 mm
$r$	0.963 mm
number of turns	1

**Table 5.12:** Optimization process 1 summary of geometric values for best solution

### 5.3.2 Optimization process 2

In the optimization process 2 a coil geometry is obtained that provides  $U_{sense} > 15 \text{ mV}$ . The parameter space allowed for the optimization parameters as well as the parameters obtained for the best solution, are shown in table 5.13 . As stopping criteria the maximum iteration number of 50 was selected. The population size was chosen to consist of 20 individuals, and 10 runs were performed.

Parameter	Min value - max value	Values for best solution of run 2	Values for best solution of run 1
$A_{sense}$	11 – 1000 $\text{mm}^2$	50.01 $\text{mm}^2$	32.22 $\text{mm}^2$
$k_x$	0.2 – 0.8	0.798	0.73
<i>curvature</i>	0 – 1	0.000431	0.09
$b_{forbidden}$	0.1 – 1	0.48	0.77

**Table 5.13:** Optimization process 2 parameter space and best obtained solution. The values of the best solution from optimization process 1 are also shown for reference.

In table 5.14 the values used for the fuzzy functions are summarized. For  $U_{sense\_min}$  the same consideration as in optimization process 1 was applied. Since  $U_{sense\_min} > 15 \text{ mV}$  a coil geometry that produces 10 % of this value is considered as a good solution and geometries with a  $U_{sense\_min} < 15 \text{ mV}$  or close to  $15 \text{ mV}$  are penalized with a high quality contribution. Due to the fact that  $U_{sense\_min}$  is increased by 50% for this optimization process, the 90% value of the fuzzy function for  $U_{pcd\_max}$  was also increased by 50%, compared to optimization process 1.

Objective	Fuzzy function value of 10%	Fuzzy function value of 90%
$U_{sense\_min}$	16.5 $\text{mV}$	15 $\text{mV}$
$U_{pcd\_max}$	0.01 $\text{mV}$	12 $\text{mV}$

**Table 5.14:** Optimization process 2 values for fuzzy functions

The behavior of the optimization parameters are shown in figure 5.14. Like for the optimization process 1,  $A_{sense}$  in figure 5.14 (a) shows a fast convergence behavior towards a small surface area. The number of turns converges towards a one turn coil, as can be seen in (e). For  $k_x$  and *curvature* shown in (b) and (c), the convergence shows a clear behavior

In figure 5.15 the behavior of the quality and the objectives are shown for all 10 runs. As for the parameters also the objectives and the quality show a fast convergence towards a narrow range of solutions.

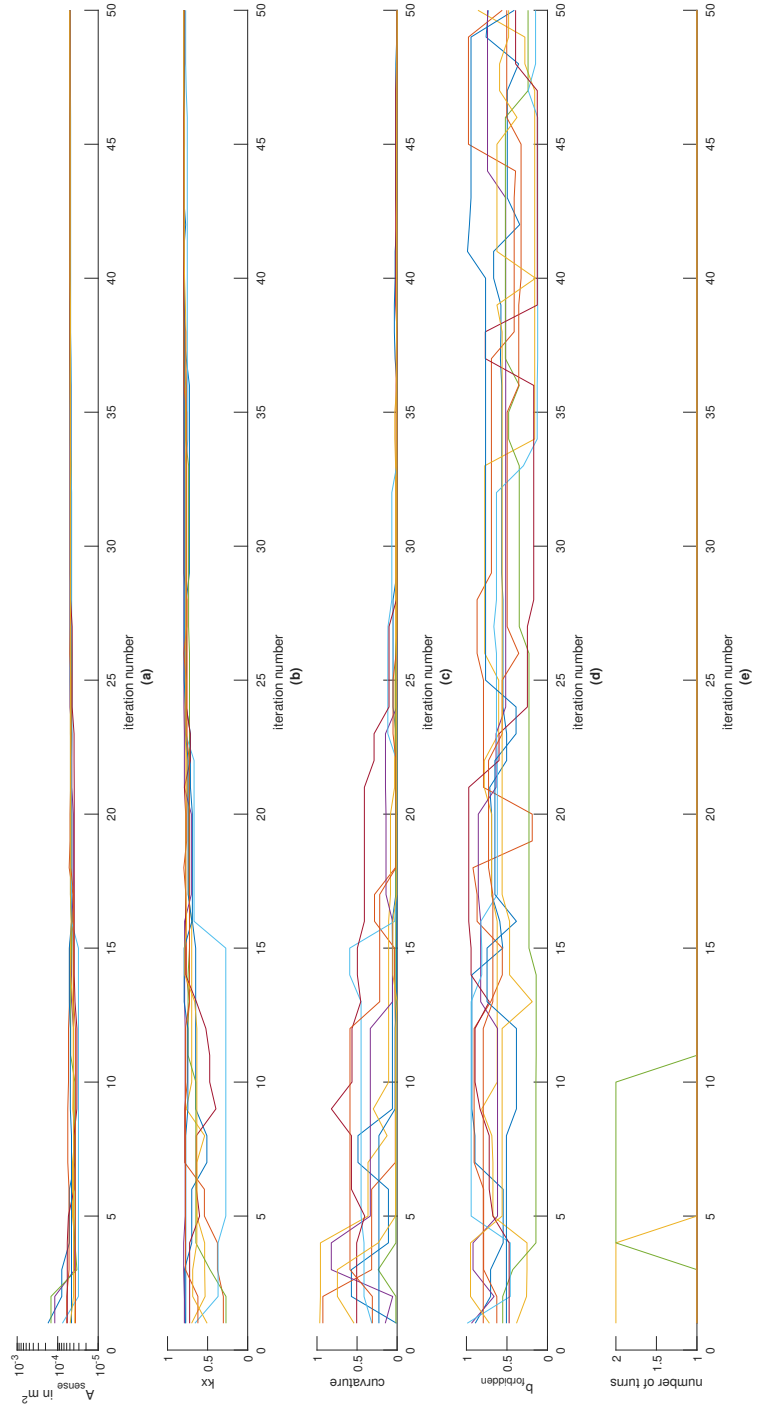


**Figure 5.14:** Optimization process 2 convergence behavior of the geometry parameters and the return value "number of turns"

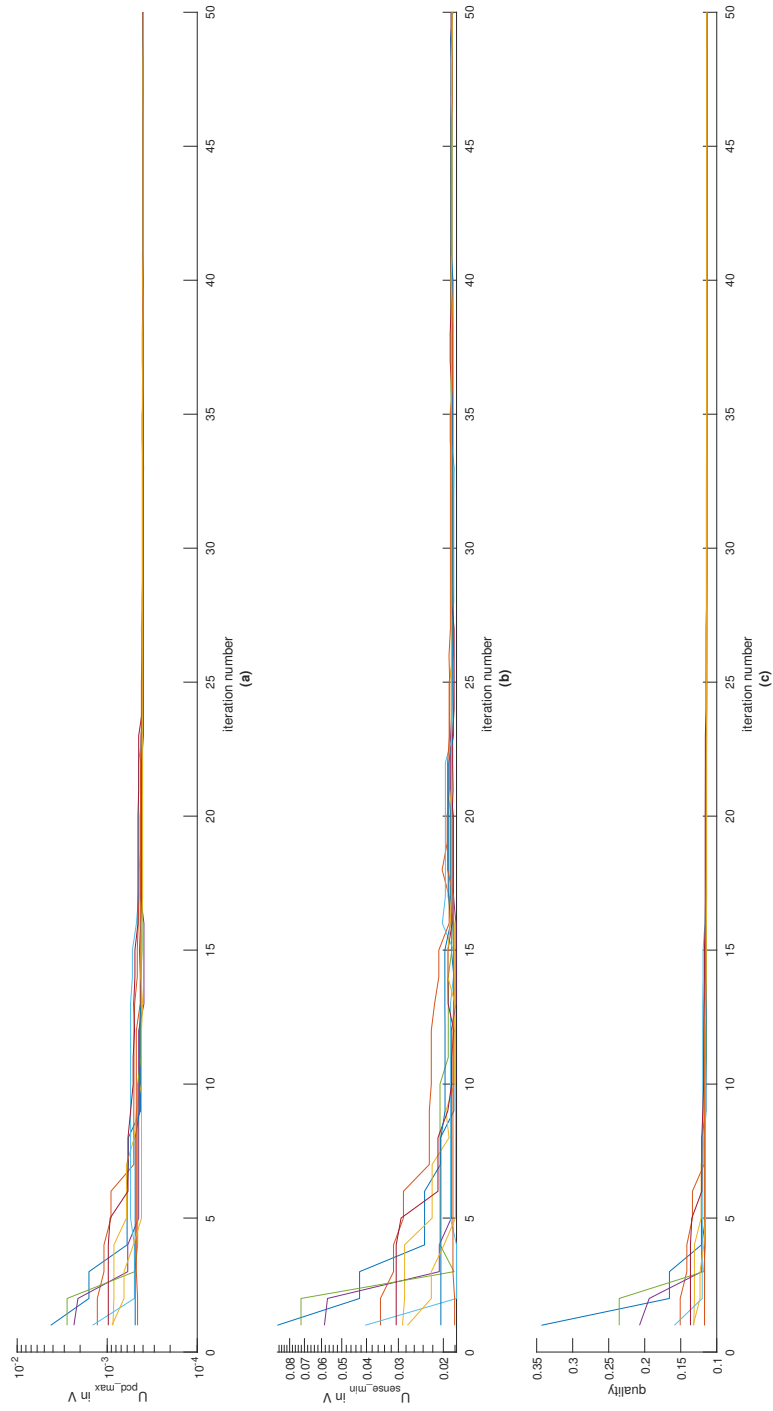
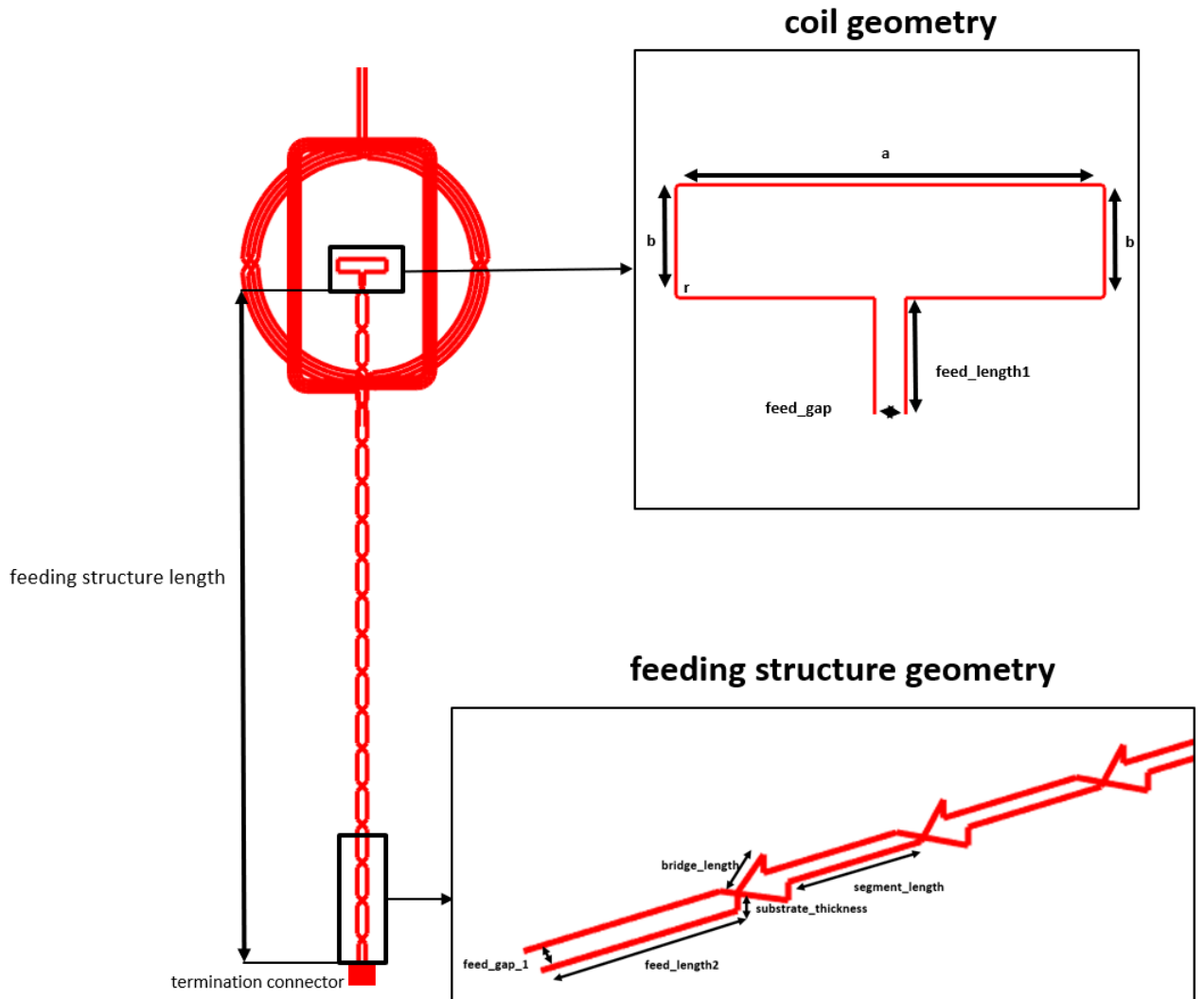


Figure 5.15: Optimization process 2 convergence behavior of objectives and quality



**Figure 5.16:** Optimization process 2 sense coil geometry for best solution

Geometric dimension	Value
$a$	13.633 mm
$b$	3.468 mm
$r$	0.083 mm
number of turns	1

**Table 5.15:** Optimization process 2 summary of geometric values for best solution

In figure 5.16 the best solution of the optimization process is shown. Due to the requirement for the coil geometry to provide  $U_{sense\_min} > 15 \text{ mV}$ , the solution is excepted to result in a bigger  $A_{sense}$  than in Optimization process 1. The optimization parameters for the best solutions of optimization process 2 are shown in table 5.13.

### 5.3.3 Voltage excitation

For the forward problem of the optimization process, the PEEC method is applied. As described in section 2.3, the PEEC method relies on a circuit interpretation of Maxwell's equations. Each stick element is described by means of lumped circuit components (see figure 2.6). Since each stick element is capacitively coupled with all other stick element as well as with the reference potential the following can be assumed: If the PEEC model is excited by means of voltage excitation the placement of the reference potential might have an effect on the computed voltage values. In order to examine this effect on the present PEEC model, voltage excitations in terms of:

- symmetrical voltage supply
- asymmetrical voltage supply
- no reference potential

are compared for circular sense coils with one turn but different radii. The results are shown in figure 5.17.

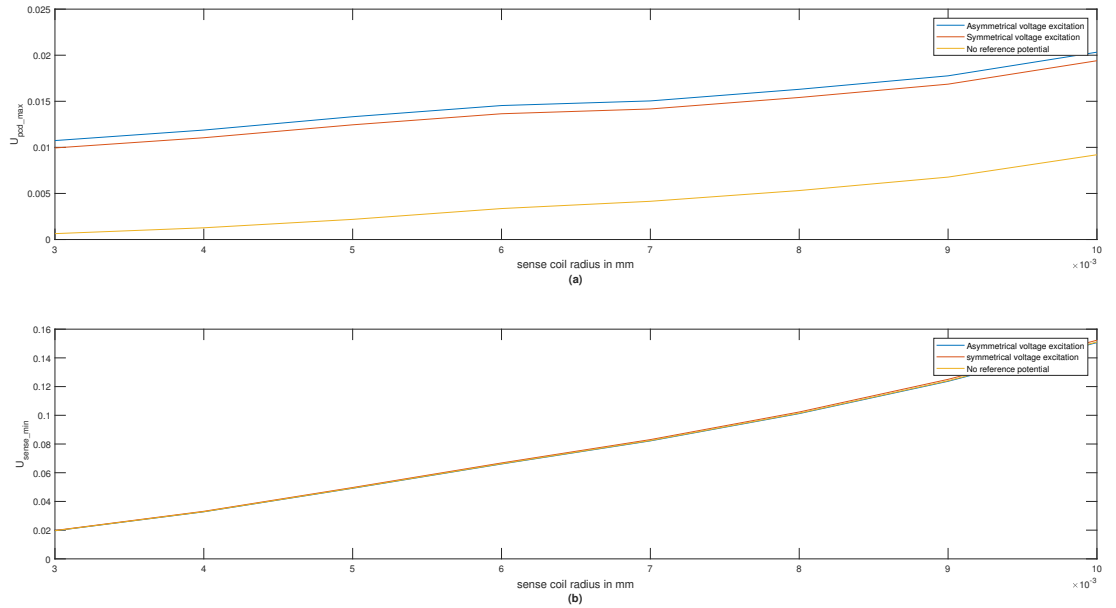


**Figure 5.17:** Comparison of different voltage excitations. (a) shows  $U_{pcd\_max}$  and (b)  $U_{sense\_min}$  of the three different voltage excitations, both with  $U_s = 3.22 V_{RMS}$ . In contrast to the optimization process where only the relevant positions of the listener in the operating volume are considered, for (a) and (b) all test positions in the EMVCo volume have been taken into account.

For  $U_{sense\_min}$  the type of the voltage excitation has only a small influence on the obtained voltage for larger coil radii, as can be seen in figure 5.17 (b). Whereas for  $U_{pcd\_max}$  in figure 5.17 (a) the obtained voltages show large deviation from each other.

Due to the fact that the voltage excitation has an influence on the obtained values for  $U_{sense\_min}$  and  $U_{pcd\_max}$ , one additional optimization process was conducted, taking the influence of the of the asymmetrical voltage excitation into account.

### 5.3.4 Optimization process 3

For optimization process 3 the voltage excitation is applied in terms of an asymmetrical voltage source. For this purpose, the reference potential is introduced at the position of the former appended node -2 (see figure 5.2). The obtained coil geometry provides  $U_{sense} > 15 \text{ mV}$  for which 25 runs were conducted with 100 iterations and 20 individuals. The parameter space allowed is the same as for the previous two optimization processes, and is shown in table 5.17. Additionally, the parameters for the best obtained solution is shown in table 5.17. In addition to the 25 runs with 100 iterations and 20 individuals, one run with 500 iterations and 20 individuals was conducted, the resulting parameters of which are also shown in table 5.17. Due to the fact that the voltage excitation was changed the evaluation of the relevant EMVCo positions was conducted, for this specific setup, resulting the test positions summarized in table 5.16

Test position	x in mm	y in mm	z in mm
TP 1	0	0	2.4
TP 2	15	0	2.4
TP 3	-15	0	2.4
TP 4	0	15	2.4
TP 5	0	-15	2.4
TP 6	15	0	42.4
TP 7	-15	0	42.4

**Table 5.16:** EMVCo test points for optimization process 3. The table shows Listener-1 positions which were taken into account during the optimization.

Parameter	Min value - max value	Values for best solution of optimization process 3	Result of the 500 iteration run
$A_{sense}$	11 – 1000 $mm^2$	31.12 $mm^2$	32.29 $mm^2$
$k_x$	0.2 – 0.8	0.71	0.72
<i>curvature</i>	0 – 1	0.34	0.49
$b_{forbidden}$	0.1 – 1	0.147	0.21

**Table 5.17:** Optimization process 3 parameter space and best obtained solution.

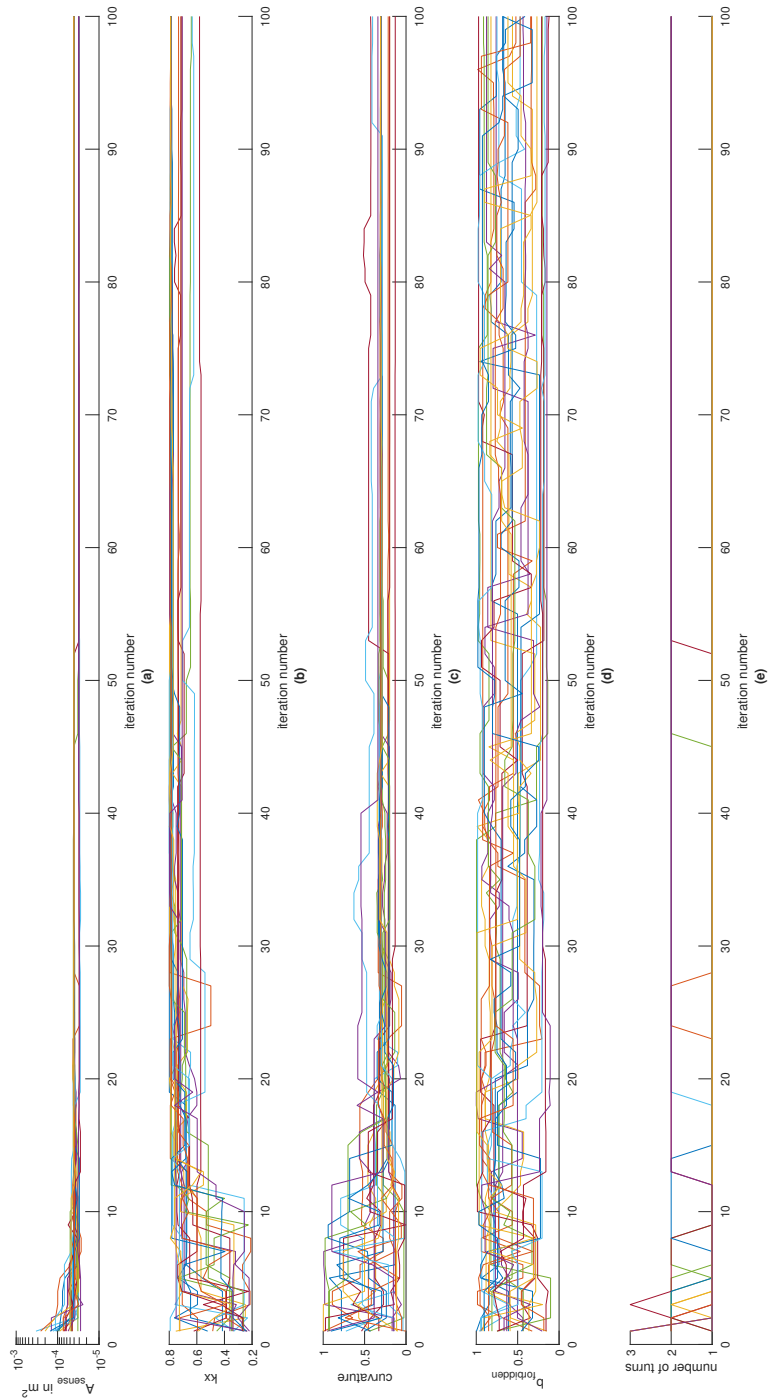
The fuzzy functions were chosen in the same manner as for optimization process 2 (see table 5.14) with the exception of the 90% value of  $U_{pcd\_max}$ . This value was selected with 16  $mV$  due to the fact that the introduction of the reference potential leads to an increased  $U_{pcd\_max}$  as discussed in subsection 5.3.3.

Figure 5.18 shows the convergence behavior of the parameters. As one can see in figure

Objective	Fuzzy function value of 10%	Fuzzy function value of 90%
$U_{sense_{min}}$	16.5 mV	15 mV
$U_{pcd_{max}}$	0.01 mV	16 mV

**Table 5.18:** Optimization process 2 values for fuzzy functions

5.18 in (e) single and dual turn solutions were reached. The single turn solutions tend towards a surface area of about  $40 \text{ mm}^2$ , whereas the two turn solutions have smaller surface areas and a better quality. However, this difference in quality is small as can be seen in figure 5.19 (c). The convergence behavior of the objectives and the quality can be seen in figure 5.19. For the convergence behavior of the parameters  $kx$  and *curvature* in figure 5.18 show a range values in which the minimum can be found. Therefore, one run with 500 iterations was conducted which resulted in a similar geometry (see table 5.17), showing that the global minimum of the optimization process results in a two turn coil.



**Figure 5.18:** Optimization process 3 convergence behavior of the geometry parameters and the return value "number of turns"

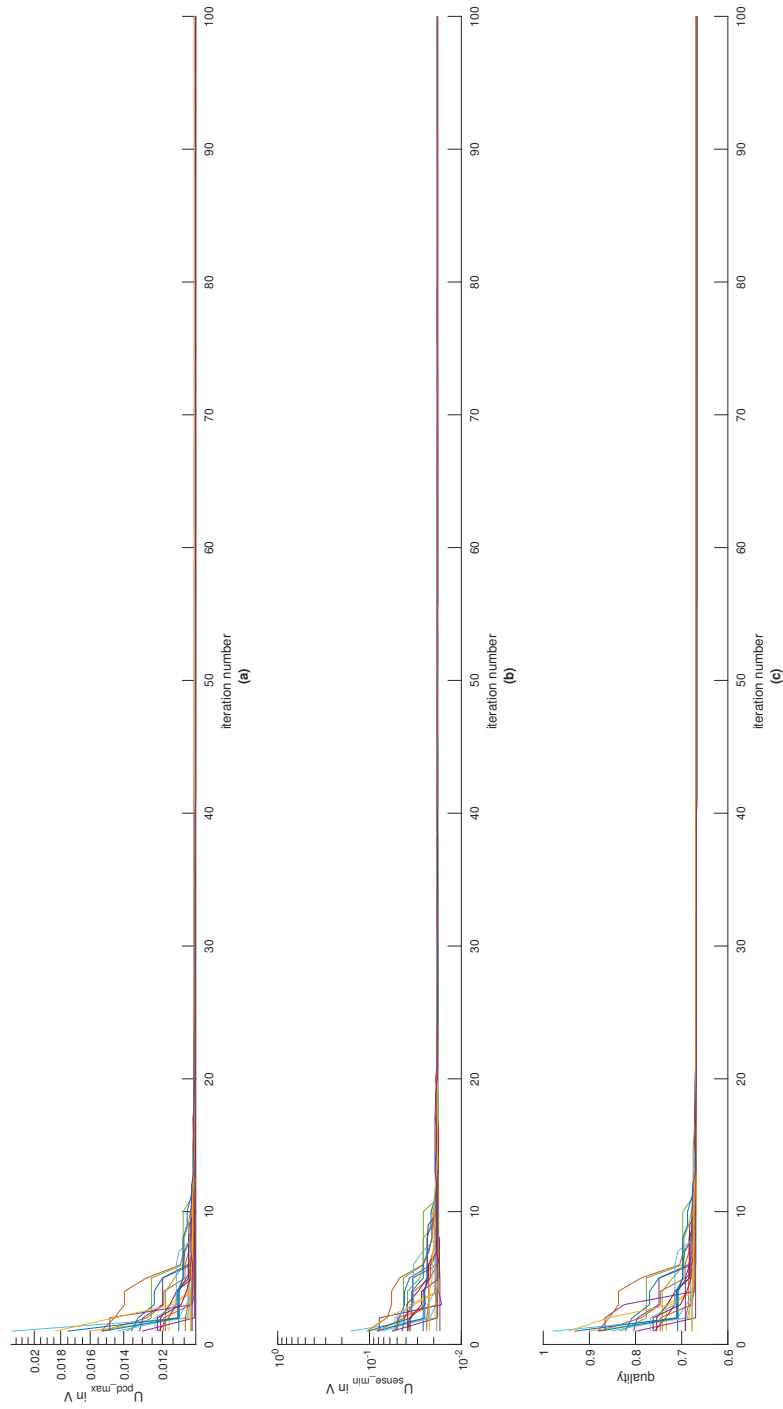
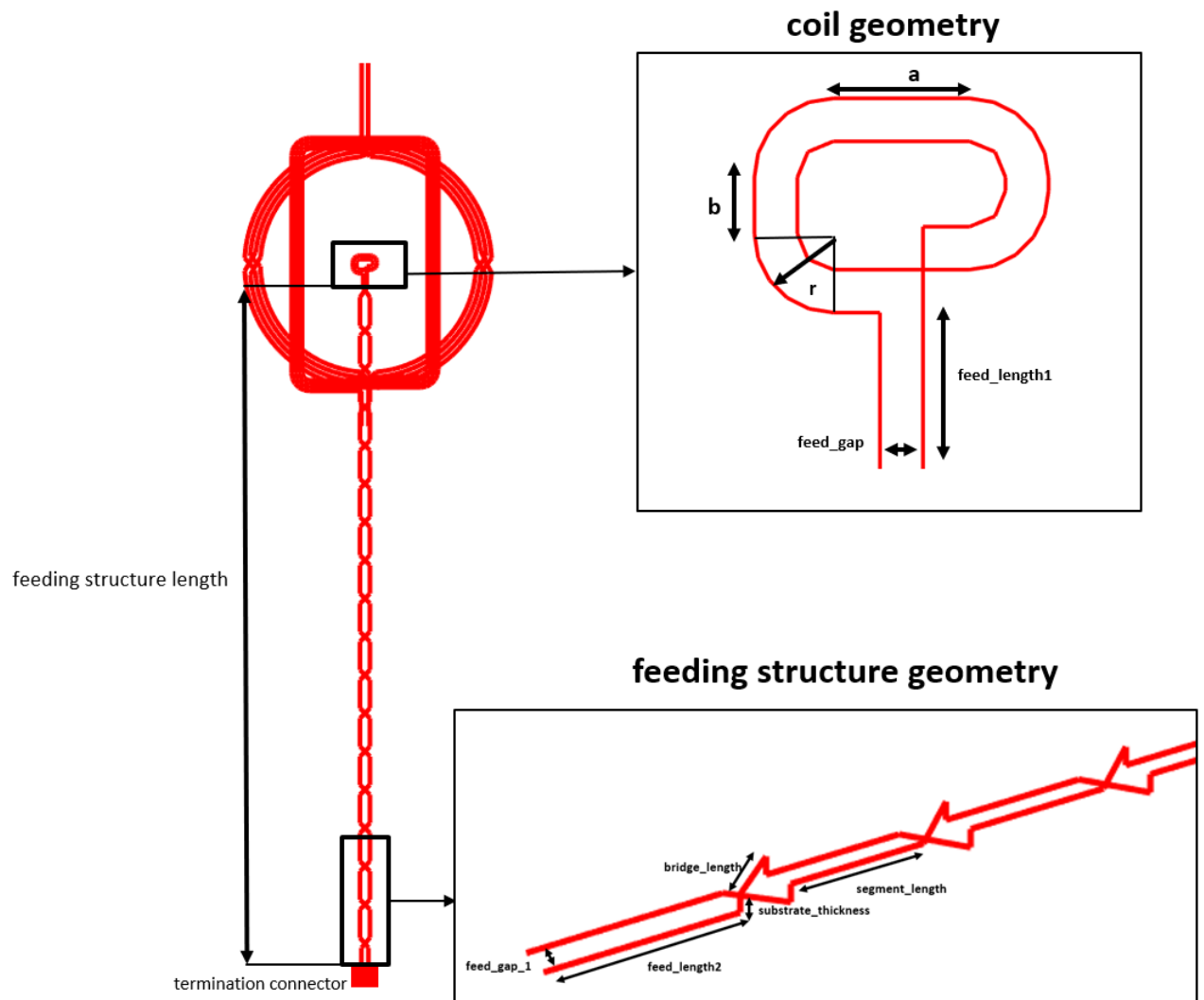


Figure 5.19: Optimization process 3 convergence behavior of objectives and quality



**Figure 5.20:** Optimization process 3 sense coil geometry for best solution

In figure 5.20 shows the best solution of optimization process 4. The solution of the 500 iteration run is not displayed, since the coil structure are similar. The coil geometry of the 500 iteration run produces a voltage of  $20.1\text{ mV}$  to the  $18.1\text{ mV}$  of the coil structure in figure 5.20. Both coil geometries, however, result in the same value for  $U_{pcd_{max}} = 10.5\text{ mV}$ . Hence, the coil geometry obtained by the 500 iteration run represents the better solution.

## Chapter 6

# Summary and outlook

In order to monitor the communication between polling devices and devices in card mode, sense coils are used which have an influence on the application environment they are measuring. Hence, it is desirable to find a measurement setup that minimizes the influence on the actual application. For this purpose a resonant system consisting of Poller-0 and Listener-1 was examined in the EMVCo operating volume. The measurement setup for the sense coil is described in section 3.4. A preliminary study was conducted for which 2D axis symmetrical simulations were performed applying "EleFAnT2D". The results of the 2D FEM simulation were then processed using MATLAB, since a direct coupling of the coil structure with the electric circuits is not implemented in the used tool. The models of Poller-0 and Listener-1 were matched and tuned according to the specifications of the NFC Forum.

The preliminary study has shown that the influence of the examined sense coil, single turn coils with radii of 10 mm, 25 mm and 40 mm, have a small effect on the resonant system, compared to the load case of Listener-1, under the condition that only the oszilloscope impedance of the measurement setup described in section 3.4 is taken into account. If, however, the whole measurement setup is considered, the effect of the sense coil becomes more noticeable for coils with a radius of 40 mm and 25 mm, depending on the Listener-1 positions. For both examinations the sense coil was assumed to be fixed at the landing plane.

In order to obtain a sense coil geometry that minimizes the influence on the resonant system of Poller-0 and Listener-1, a DE optimization strategy which uses PEEC models of Poller-0, Listener-1 to formulate the forward problem as described in section 5.2 was applied. The implementation of the PEEC is based on 1-dimensional stick elements which assume a constant current density at each stick element. Hence, no skin or proximity effects can be taken into account.

For Listener-1 the load case of Hmin was assumed and all the test points of the EMVCo operating volume were considered. In order to reduce the computational effort, the positions in the EMVCo operating volume which are relevant for the optimization process were determined. This reduces the computational effort by a factor of 5.2 for optimization process 3 and a factor of 6.2 for optimization processes 1 and 2. The values of the

objectives which were logged during the optimization process did not correspond to the obtained quality. Due to an error which unfortunately could not be located, the objectives values were recalculated after the optimization process. The recalculated objective values correspond to the obtained quality during the optimization process. Hence, it is assumed that this effect has no influence on the convergence of the parameters.

The first two optimization processes are based on a voltage excitation considering no reference potential. In the applied implementation, the reference potential is assumed to be placed in infinity in such a case. With two optimization processes sense coil geometries which produce a sense coil voltage of  $U_{sense} > 10 \text{ mV}$  and  $U_{sense} > 15 \text{ mV}$  respectively were obtained. One additional optimization process was conducted (optimization process 3), taking the reference potential of the voltage excitation into account, obtaining a coil geometry that produces a sense coil voltage of  $U_{sense} > 15 \text{ mV}$ . Due to the fact that each stick element is coupled capacitively to the ground potential, the introduction of the reference potential has an influence on the coil geometry. By comparing the obtained geometry of both optimization processes in which the sense coil produces  $U_{sense} > 15 \text{ mV}$  (see figure 5.16 and figure 5.20) this characteristic can be observed. Hence, by taking the reference potential of the oscilloscope into account, the obtained objectives are expected to change. Therefore, the objectives of the coil geometry shown in figure 5.20 are computed taking the reference potential of the oscilloscope into account. The the obtained objectives are the following:

- $U_{sense_{min}} = 12.4 \text{ mV}$
- $U_{pcd_{max}} = 27.6 \text{ mV}$

By taking only the reference potential of the voltage supply into consideration, the following objectives were obtained:

- $U_{sense_{min}} = 18.1 \text{ mV}$
- $U_{pcd_{max}} = 10.5 \text{ mV}$

Hence, the consideration of the reference potential of the oscilloscope results in a decrease in coil sense coil voltage and an increase in  $U_{pcd_{max}}$ . In reality, connecting an unbalanced device, such as an oscilloscope directly to a balanced sense coil, results in a mode mismatch at the antenna terminals. This, in turn, causes coating currents which lead to a deterioration of the measurement data [8]. There are a couple of options to prevent coating currents. First, a galvanic separated oscilloscope or voltage supply could be used. Secondly, the coil geometry of the sense coil could be electrically compensated. However, this would likely result in higher influence on the resonant system of Poller-0, since the conducting material required for the coil geometry increases, and hence the parasitic capacitance increases too.

The coil geometries obtained represent an optimal coil geometry for the specific setup for which it was synthesized. Hence, if the obtained sense coil is used for measuring NFC systems with different coil geometries, the results can not be predicted. A more general geometry could be obtained by using different reference coils in the optimization process. One natural choice for this would be to use all NFC Forum reference poller and listener devices in each permutation. However, this would result in a high computational effort since more coil setups have to be calculated.

Another aspect for future research is mounting the sense coil below Listener-1. This sense coil placement could be beneficial for automatic test procedures. However, test runs have shown that the number of test points for such a sense coil placement can not be efficiently reduced, as was done for the optimization processes 1 to 3. This is due to the fact that compared to the stationary placement of the sense coil, far more critical positions (positions in which  $U_{pcd_{max}}$  and  $U_{sense_{min}}$ ) occur. Hence, the entire test points in the EMVCo volume is required to be taken into account. This in turn results in very high computational effort. Therefore, this sense coil placement was not further investigated but is an interesting topic for future research.

# Bibliography

- [1] NFC Forum, "Analog Technical Specification", Version 2.1, 2018.
- [2] P. G. Alotto, C. Eranda, B. Brandstätter, G. Fprntratt, C. Magele, G. Molinari, M. Nervi, K. Preis, M. Repetto, and K. R. Richter, "Stochastic Algorithms in Electromagnetic Optimization," IEEE TRANSACTIONS ON MAGNETICS, VOL. 34, NO. 5, 1998.
- [3] P. Alotto, "A hybrid multiobjective differential evolution method for electromagnetic device optimization," [https://www.researchgate.net/publication/229211220\\_A\\_hybrid\\_multiobjective\\_differential\\_evolution\\_method\\_for\\_electromagnetic\\_device\\_optimization](https://www.researchgate.net/publication/229211220_A_hybrid_multiobjective_differential_evolution_method_for_electromagnetic_device_optimization), 2011, accessed Jan 28, 2020.
- [4] T. Bauernfeind, P. Baumgartner, O. Biro, C. Magele, W. Renhart, and R. Torchio, "PEEC-Based Multi-Objective Synthesis of NFC Antennas in the Presence of Conductive Structures," IEEE TRANSACTIONS ON MAGNETICS, VOL. 54, NO. 3, March 2018.
- [5] S. McHugh and K. Yarmey, "Near Field Communication Recent Developments and Library Implications," MORGAN & CLAYPOOL PUBLISHERS, 2014, pp. 5.
- [6] K. Finkenzyler, *RFID Handbook*. Sussex England: John Wiley and Sons Ltd, 2003.
- [7] ISO IEC, "ISO IEC 14443-2," 2017, pp. 12.
- [8] T. Bauernfeind, K. Preis, W. R. O. Biro, and M. Gebhart, "Finite Element Simulation of Impedance Measurement Effects of NFC Antennas," IEEE TRANSACTIONS ON MAGNETICS, VOL. 51, NO. 3, March 2015.
- [9] J. W. Nilsson and S. A. Riedel, "Electric Circuits," Pearson Education Inc., 2008.
- [10] H. Fricke and P. Vaske, "Elektrische Netzwerke, Grundlagen der Elektrotechnik Teil 1," Springer Fachmedien Wiesbaden, 1982.
- [11] W. Klein, *Vierpoltheorie*. Mannheim Deutschland: Bibliographisches Institut AG, 1972.
- [12] J. W. Nilsson and S. A. Riedel, "Electric Circuits," Pearson Education Inc., 2015.
- [13] J. Ekman, "Electromagnetic Modeling Using the Partial Element Equivalent Circuit Method," Ph.D. dissertation, Dept. of Computer Science and Electrical Engineering Luleå University of Technology, Sweden, 2003.

- [14] A. E. Ruehli, "Equivalent Circuit Models for Three-Dimensional Multiconductor Systems," March 1974, IEEE TRANSACTIONS ON MICROWAVE THEORY AND TECHNIQUES, VOL. MTT-22, No.3.
- [15] G. Antonini, "The Partial Element Equivalent Circuit Method for EMI, EMC and SI Analysis," [https://www.researchgate.net/publication/289256382\\_The\\_partial\\_element\\_equivalent\\_circuit\\_method\\_for\\_EMI\\_EM\\_C\\_and\\_SI\\_analysis](https://www.researchgate.net/publication/289256382_The_partial_element_equivalent_circuit_method_for_EMI_EM_C_and_SI_analysis), March 2006, accessed Feb 07, 2020.
- [16] T. Bauernfeind, P. Baumgartner, O. Biro, C. Magele, K. Preis, and R. Torchio, "PEEC-Based Multi-Objective Synthesis of Non-Uniformly Spaced Linear Antenna Arrays," IEEE TRANSACTIONS ON MAGNETICS, VOL. 53, NO. 6, June 2017.
- [17] T. Bauernfeind, P. Baumgartner, O. Biro, A. Hackl, C. Magele, W. Renhart, and R. Torchio, "Multi-objective synthesis of nfc-transponder systems based on peec method," IEEE TRANSACTIONS ON MAGNETICS, VOL. 54, NO. 3, March 2018.
- [18] EMVCo, "PCD Analogue Test Bench and Test Case Requirements," 2013, Version 2.3.1a.
- [19] A. Mantzke and M. Leone, "Novel Equivalent-Circuit Model for Electrically Short Transmission Lines Including Field Coupling," IProc. of the 2017 International Symposium on Electromagnetic Compatibility , September 2017.
- [20] C. A. Tucker, U. Muehlmann, and M. Gebhart, "Contactless power transmission for NFC antennas in credit-card size format," IET Journals, IET Circuits, Devices & Systems, Feb 2016, ISSN 1751-858X.
- [21] T. Bauernfeind, P. Baumgartner, O. Biro, C. Magele, W. Renhart, and R. Torchio, "PEEC-Based Multi-Objective Synthesis of NFC Antennas in the Presence of Conductive Structures," ACES JOURNAL, Vol. 34, No 2, February 2019, 2019.
- [22] NFC Forum, "Reference Equipment Verification Tests", Version 1.0.12, 2014.
- [23] W. Klein, *Mehrtortheorie*. Darmstadt Deutschland: Akademie-Verlag Berlin, 1976.
- [24] C. Koger, "Optimierung von NFC Antennen," 2018, bachelor thesis, Graz university of technology, Institute of Fundamentals and Theory in Electrical Engineering.